ESTCP

FINAL REPORT

Field-Scale Demonstration of a Novel Real-Time Sensor for PFAS

A Novel Real-Time PFAS Sensor with High Selectivity and Sensitivity

Craig Divine
Jeffrey McDonough
Vivek Pulikkal
Arcadis

Radha Kishan Motkuri
Dushyant Barpaga
Gabriel Hall
Pacific Northwest National Laboratory

Jovan Popovic
NAVFAC EXWC

Marlowe Laubach
USACE

Sagnik Basuray
New Jersey Institute of Technology

September 2023

ESTCP Project ER21-5101

REPORT DOCUMENTATION PAGE

Form Approved
OMB No. 0704-0188

1. REPORT DATE *(DD-MM-YYYY)*	**2. REPORT TYPE**	**3. DATES COVERED** *(From - To)*
30/09/2023	ESTCP Final Report	10/15/2021 - 10/14/2025

4. TITLE AND SUBTITLE

Field-Scale Demonstration of a Novel Real-Time Sensor for PFAS

A Novel Real-Time PFAS Sensor with High Selectivity and Sensitivity

5a. CONTRACT NUMBER
22-C-0003

5b. GRANT NUMBER

5c. PROGRAM ELEMENT NUMBER

6. AUTHOR(S)

Craig Divine, Jeffrey McDonough and Vivek Pulikkal: Arcadis

Radha Kishan Motkuri, Dushyant Barpaga and Gabriel Hall: Pacific Northwest National Laboratory

Jovan Popovic: NAVFAC EXWC

Marlowe Laubach: USACE

Sagnik Basuray: New Jersey Institute of Technology

5d. PROJECT NUMBER
ER21-5101

5e. TASK NUMBER

5f. WORK UNIT NUMBER

7. PERFORMING ORGANIZATION NAME(S) AND ADDRESS(ES)
Arcadis US, Inc.
320 Commerce, Suite 200
Irvine, CA 92602

8. PERFORMING ORGANIZATION REPORT NUMBER
ER21-5101

9. SPONSORING/MONITORING AGENCY NAME(S) AND ADDRESS(ES)
Office of the Deputy Assistant Secretary of Defense (Energy Resilience & Optimization)
3500 Defense Pentagon, RM 5C646
Washington, DC 20301-3500

10. SPONSOR/MONITOR'S ACRONYM(S)
ESTCP

11. SPONSOR/MONITOR'S REPORT NUMBER(S)
ER21-5101

12. DISTRIBUTION/AVAILABILITY STATEMENT
DISTRIBUTION STATEMENT A. Approved for public release: distribution unlimited.

13. SUPPLEMENTARY NOTES

14. ABSTRACT
The novel Per- and polyfluoroalkyl substances (PFAS) electrochemical sensor was developed collaboratively at the Pacific Northwest National Laboratory and New Jersey Institute of Technology. The intended application of this sensor is to use at downstream of PFAS treatment systems at DoD sites to measure PFAS concentrations with high selectivity and sensitivity. The flow-through electrochemical sensor uses a nanoporous and capacitive electrode technology based on NP-μFEC to detect and quantify PFAS. The overarching goal of this project was to field-validate the use of a portable electrochemical sensor technology for rapid assessment of PFAS at DoD sites. Originally, objectives for this project included evaluating the sensor performance with six PFAS in synthetic samples, studying sample interference and field-testing the sensor at downstream of a DoD PFAS treatment system.

15. SUBJECT TERMS
Novel Real-Time PFAS Sensor, PFAS, High Selectivity and Sensitivity, Sampling and Analysis

16. SECURITY CLASSIFICATION OF:			**17. LIMITATION OF ABSTRACT**	**18. NUMBER OF PAGES**	**19a. NAME OF RESPONSIBLE PERSON**
a. REPORT	**b. ABSTRACT**	**c. THIS PAGE**			Craig Divine
UNCLASS	UNCLASS	UNCLASS	UNCLASS	51	**19b. TELEPHONE NUMBER** *(Include area code)* 720-308-5367

FINAL REPORT
Project: ER21-5101

TABLE OF CONTENTS

Page

LIST OF FIGURES

Page

LIST OF FIGURES

Page

LIST OF TABLES

Page

ACRONYMS AND ABBREVIATIONS

AFFF	Aqueous Film Forming Foams
CNT	Carbon Nanotube
COF	covalent organic framework
DOC	dissolved organic carbon
EIS	Electrical Impedance Spectroscopy
ELAP	Environmental Laboratory Accreditation Program
ESSENCE	electrochemical sensing shear-enhanced, flow-through, nanoporous and capacitive electrode
ESTCP	Environmental Security Technology Certification Program
HAL	health advisory level
HPC	hierarchical porous carbons
LC-MS/MS	liquid chromatography with tandem mass spectrometry
M	Molar
MCL	maximum contaminant level
MOF	metal-organic framework
ng/L	nanograms per liter
NJIT	New Jersey Institute of Technology
NMR	nuclear magnetic resonance
NP-IDμE	nonplanar interdigitated microelectrode
PBS	phosphate-buffered saline
PFAS	per- And polyfluoroalkyl substances
PFBS	perfluorobutane sulfonic
PFOA	perfluorooctanoic acid
PFOS	perfluorooctane sulfonate
PNNL	Pacific Northwest National Laboratory
QC	quality control
RSD	relative standard deviation
SERS	Surface Enhanced Raman Spectroscopy
SNR	signal to noise ratio
SPR	Surface Plasmon Resonance
USEPA	United States Environmental Protection Agency

ACKNOWLEDGEMENTS

This work was completed with critical support from the following individuals:

- Dr. Zhenglong Li (NJIT)
- Dr. Abhisek Kumar (PNNL, Synthesis, Characterization, Testing)
- Mr. Joshua Torgeson (PNNL, Testing)
- Mr. Julian Schmid (PNNL, Synthesis, Characterization)
- Dr. Victor Aguilera-Vazquez (PNNL, Clean Room, Device Fabrication)
- Dr. Hardeep Mehta (PNNL, Clean Room, Device Fabrication)

ABSTRACT

The novel Per- and polyfluoroalkyl substances (PFAS) electrochemical sensor was developed collaboratively at the Pacific Northwest National Laboratory (PNNL) and New Jersey Institute of Technology (NJIT). The intended application of this sensor is to use at downstream of PFAS treatment systems at DoD sites to measure PFAS concentrations with high selectivity and sensitivity. The flow-through electrochemical sensor uses a nanoporous and capacitive electrode technology based on NP-μFEC to detect and quantify PFAS. The overarching goal of this project was to field-validate the use of a portable electrochemical sensor technology for rapid assessment of PFAS at DoD sites. Originally, objectives for this project included evaluating the sensor performance with six PFASs in synthetic samples, studying sample interference and field-testing the sensor at downstream of a DoD PFAS treatment system.

The detection of perfluorooctane sulfonate (PFOS) in spiked tap water solutions was demonstrated with separate sensors, one based on Cr-MIL-101 and other on Fe-MIL-101. These two MOFs showed high PFOS uptake during sorption studies conducted at PNNL with Fe-MIL-101 outperforming Cr-MIL-101. The sensor housing Cr-MIL-101 was evaluated at six different PFOS concentrations of 10, 25, 50, 75, 100 and 150 ng/L. The initial results were promising with the sensor detecting the lowest standard of 10 ng/L. Even though a linear relation between the PFOS concentration and normalized sensitivity was obtained, the large standard deviations among detections at each concentration overlapped with most other standards. Furthermore, statistical analyses indicated low confidence in this correlation. Tests using sensors that housed Fe-MIL-101 showed better sensitivity compared to Cr-MIL-101. Using Fe-MIL-101, detections at 1, 10 and 50 ng/L PFOS solutions were carried out. A linear relationship between concentration and normalized sensitivity was obtained, but similar to Cr-MIL-101 the standard deviations at each concentration overlapped with others.

Detection of perfluorooctanoic acid (PFOA) in spiked tap water solutions was demonstrated using separate sensors that housed UIO-66 and UIO-66-NH2 at PFOA concentrations of 10, 50, 100, 500 and 1000 ng/L. These two MOFs were selected based on their high PFOA uptake observed during sorption studies conducted at PNNL. A linear relationship between PFOA concentrations and normalized sensitivity was not obtained possibly due to the inability to lower the particle size of UIO-66 and UIO-66-NH2 resulting in packed channels of relatively high porosity in the sensor. Loosely packed MOFs in the sensor could cause electrical charges to transfer to the external circuit through other pathways resulting in erroneous sensitivity readings. Additionally, the sensor showed high sensitivity even in blank samples which overlapped with sensitivities obtained for all other samples including the highest PFOA standard of 1000 ng/L. Tests using Cr-MIL-101 based sensors for PFOA showed poor selectivity between PFOA and PFOS. The selectivity and performance of the sensor in PFAS mixtures could be improved by using MOFs with high affinity for the target PFASs and adopting multiple sensors in series and parallel configuration as show in Figure 4.1.

The high variation in sensitivity readings and false positives in blanks warranted further investigation. To address this, Arcadis coordinated a double-blind QC test to assess the precision and accuracy of the PFAS sensor. Nine PFOS standards including a DI water blank were sent to NJIT for sensor testing and to Pace Analytical lab for validation. Nine standards included one DI water blank, five at a PFOS concentration of 47 ng/L, two at 15 ng/L, and the remaining one standard at 75 ng/L.

The sensor results were compared to the Pace lab results to arrive at the accuracy and precision values of the sensor. The PFAS sensor results for the 47 ng/L PFOS standard ranged from 102 to 580.7 ng/L which was 429 to 2420% of the concentration reported by Pace lab (24 ng/L). Precision of the sensor was at a %RSD of 83% among the five sensor readings. For the 75 ng/L PFOS standard, the PFAS sensor showed a result of 117.3 ng/L which was 267% of the Pace lab result (44 ng/L) and had a standard deviation of 52 ng/L. Finally, the sensor showed a PFOS concentration of 140.7 ng/L for the DI water blank while Pace lab did not detect any PFOS in it. Based on the results, the accuracy and precision of the sensor deviated substantially from the accuracy precision performance goals for the sensor.

Parallelly, a study was conducted to evaluate the MOF variability between different batches and a method to get a uniform particle distribution across different batches was developed. However, previous tasks that evaluated the PFAS sensor used MOFs from different batches. Interestingly the electrochemical behavior between the two batches were found to be different which made translating the calibration curve from one batch of MOF to another challenging. All these challenges along with the significant challenge of achieving uniform chip packing and variable accessibility to MOF sorption sites. Currently, the chips are single use and packed manually. Moreover, the small size of the sensors makes uniform packing challenging. Because of this, MOF sorption behavior varies significantly from chip to chip.

In conclusion, the precision goals cannot be achieved under the manual fabrication method. To avoid chip to chip to variation in the future, a larger chip design with automated packing needs to be adopted. However, this will likely require complete chip redesign and different chip production equipment which the team currently does not have access to. Moreover, this will require significant additional bench testing and troubleshooting which are beyond the scope of this project. Hence, a No-Go was recommended for the remaining project tasks.

EXECUTIVE SUMMARY

INTRODUCTION

Per- and polyfluoroalkyl substances (PFASs) are a group of anthropogenic chemicals that have demonstrated high persistence due to their physical and chemical properties. Among their many applications, their use in Aqueous Film Forming Foams (AFFF) has resulted in groundwater and soil impacts at DoD sites. Comparatively low regulatory screening levels for PFAS have created a need for fast, reliable, and cost-effective measurement. The PFAS electrochemical sensor is an adaptable technology that will be integrated into a broad range of applications, such as initial characterization and remedy evaluation. Compared to conventional PFAS analysis, the novel PFAS sensor has advantages including faster PFAS measurements, low cost per sample, and similar selectivity and sensitivity.

This Final Report (report) describes the bench scale demonstration and performance assessment associated with ESTCP Project ER21-5101, which bench-tested the novel PFAS sensor. The overarching goal of this demonstration was to field-validate a novel real-time PFAS sensor for use at downstream of PFAS treatment systems at DoD sites to measure PFAS concentrations with high selectivity and sensitivity. Specific objectives included:

i. Quantify PFAS sensor performance (i.e., accuracy, precision, sensitivity) in laboratory prepared PFAS standards with comparison to an Environmental Laboratory Accreditation Program (ELAP)-accredited laboratory. The goal is to attain an accuracy similar to the ELAP certified laboratory and a precision ≤30%.
ii. Quantify PFAS sensor performance in representative field samples with comparison to an ELAP accredited laboratory. The comparison will be made by submitting split samples (n ≥ 3 for each sample tested) to an ELAP-accredited laboratory for analysis by either PFAS by LC-MS/MS (according to Table B-15 of DoD QSM 5.3 [or latest version]) or by EPA method 533.
iii. Identify sensor configuration adjustments for field application and any limitations for use with field samples (e.g., geochemical or co-contaminant interferences).
iv. Demonstrate a field-deployable sensor configuration for a PFAS water treatment and/or monitoring application. PFAS sensor performance will be evaluated onsite by comparison of sensor measurements with laboratory-based analysis. The comparison will be made by submitting split samples (n ≥ 3 for each sample tested) to an ELAP-accredited laboratory for analysis by either PFAS by LC-MS/MS (with DoD QSM 5.3 [or latest version] compliance) or by EPA method 533. Technology transfer will be initiated following successful completion of field demonstration.

TECHNOLOGY DESCRIPTION

The microfluidic platform design as well as its integration with the engineered nanoporous materials for detection and quantification of PFAS targets has been developed in collaboration between PNNL and NJIT. The new electrochemical sensor utilizes a new electrochemical sensing shear-enhanced, flow-through, nanoporous and capacitive electrode (ESSENCE) technology based on a nonplanar interdigitated microelectrode (NP-IDμE) array described below.

The schematics of PFAS detection are shown in Figure ES-1. The NP-IDμE device (shown on Figure ES-2) consists of three layers, a top and bottom IDμE and a middle adsorptive layer. The adsorptive probe can be based on porous MOFs, zeolites, covalent organic frameworks (COFs) or hierarchical porous carbons (HPCs). The focus on these adsorbent probes is based on recent observations by PNNL (Motkuri et al., 2014, Bower et al., 2018, Barpaga et al., 2019a, Zheng et al., 2018, Zheng et al., 2017, Zheng et al., 2020) and elsewhere (Chen et al., 2016, Liu et al., 2015, Sini et al., 2018, Ji et al., 2018) of their superfluorophilicity, which allows the separation of perfluoroalkyl chains from other organics. PNNL and NJIT have previously validated the use of a MOF (such as Cr-MIL-101) associated with Carbon Nanotubes (CNTs) for its performance towards selective capture of PFAS. Initial data suggest that the use of ESSENCE technology will boost both sensitivity and selectivity while mitigating fouling and decrease artifacts in the measurable signal.

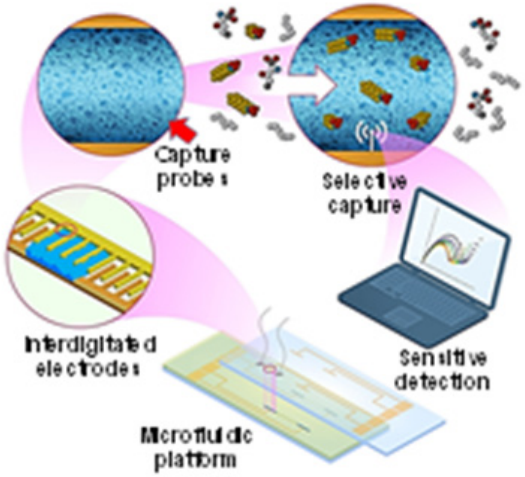

Figure ES-1. Schematics of PFAS Detection

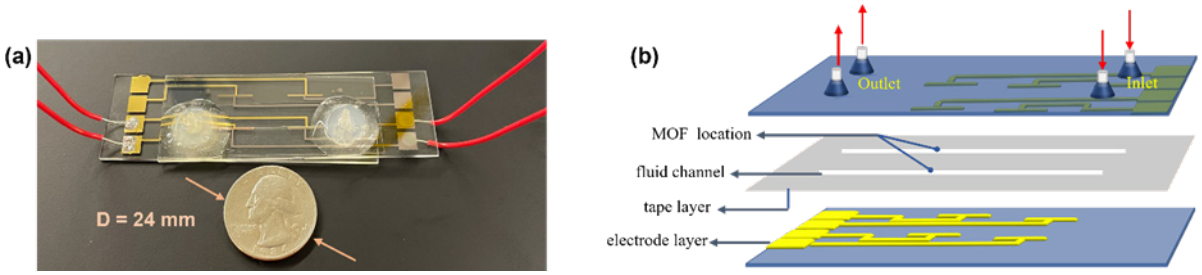

Figure ES-2. (a) Image Showing MOF-packed NP-μFEC (b) Schematic Diagram if Blank NP-μFEC

PERFORMANCE ASSESSMENT

A comparison of PFOS capture on four MIL-type materials, Cr-MIL 101, Fe-MIL-101, Fe-MIL-100, and Fe-MIL-88b, at levels near and below EPA health advisory levels (parts per trillion, ppt) as well as at levels as high as 10 mM (parts per million, ppm) were conducted to study the uptake capacity of these MOFs. Both Fe-MIL-100 and Fe-MIL-101 showed high sorption capacities, while Cr-MIL-101 showed saturation (Fig. ES-3). UiO based MOFs were tested for PFOA sorption.

These MOFs showed have shown favorable conditions for the PFOA capture in water is the zirconium-based UiO-type framework. A series of zirconium-based UiO-66-based MOFs, such as UiO-66, UiO-66-NH_2, UiO-66-$(OH)_2$, UiO-66-$(COOH)_2$, and UiO-66-F_4 were synthesized, characterized and tested for PFOA capture at ppm levels. The results showed UiO-66 and its F_4 substituted material to have high PFOA sorption capacities (Figure ES-4).

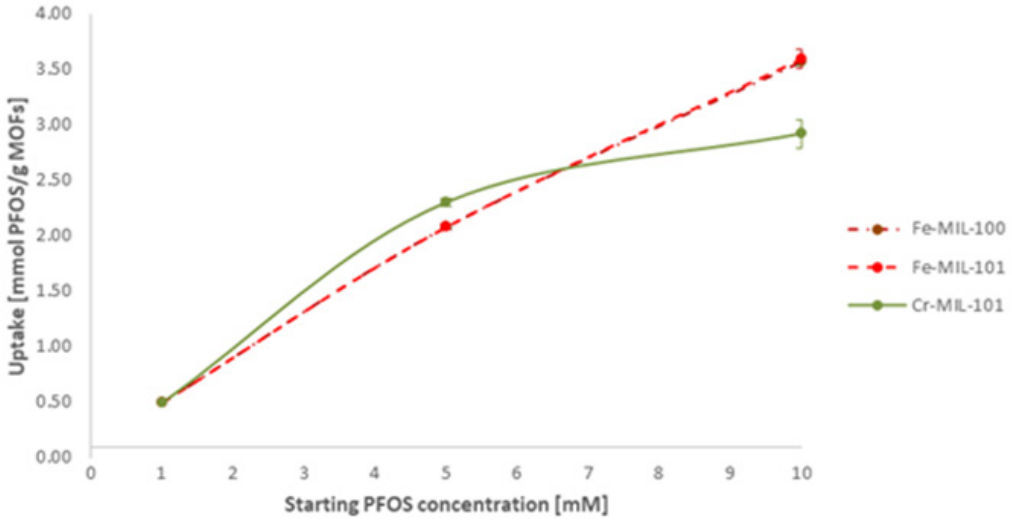

Figure ES-3. PFOS Capture at ppm Levels in MIL Family of MOFs

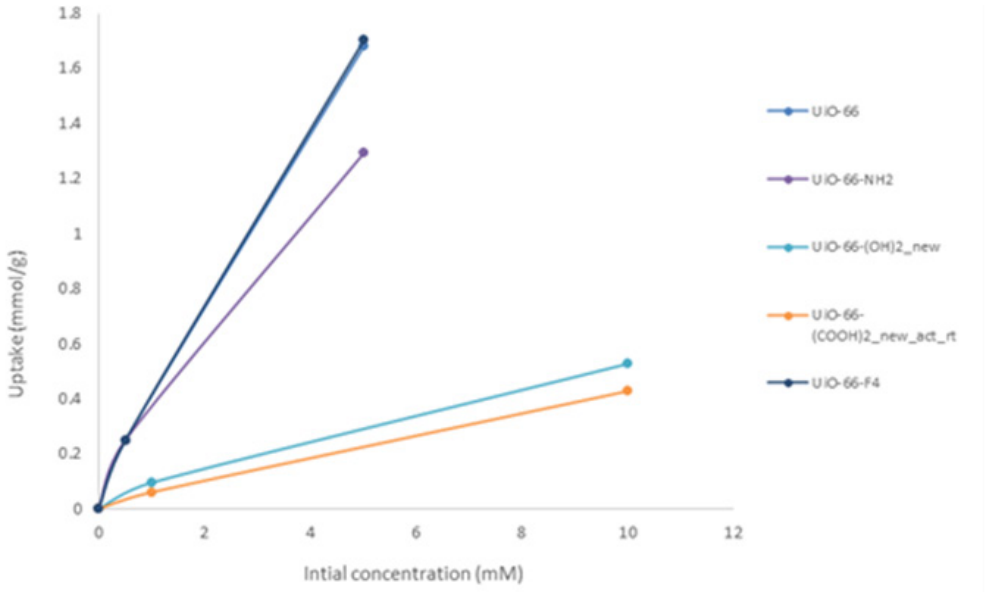

Figure ES-4. PFOA Capture at ppm Levels in the UiO-66 Family of MOFs

PFAS sensor performance (i.e., accuracy, precision, sensitivity) was assessed and optimized in PFAS standards and calibration curves were generated based on the sensor's sensitivity at different concentrations. The task was designed to include testing the sensor performance in tap water solutions spiked with individual PFASs. The six PFASs targeted in this study are PFOS, PFOA, PFHxA, PFHxS, PFBA and PFBS. Each PFAS compound was intended to be tested individually for concentrations ranging from 10 to 150 ng/L and the sensor's normalized sensitivity to different PFAS concentrations will be developed. Detection of PFOS in tap water solutions was demonstrated using NP-μFEC. Cr-MIL-101 and Fe-MIL-101 have been used as transducer materials for the sensor to evaluate their characteristic as potential materials for selectivity and sensitivity. Six different PFOS concentrations (10, 25, 50, 75, 100, and 150 ng/L) have been tested, and relevant results are presented in Figure 2. Cr-MIL-101 for PFOS tap water analysis is completed. For the analysis, the EIS data from 1.2 kHz to 100 MHz was fitted using the Randall equivalent circuit and using EIS software Zsigmawin. As can be seen from Figure ES-5 and Figure ES-6, Fe-Mil-101 shows higher sensitivity for PFOS than Cr-Mil-101.

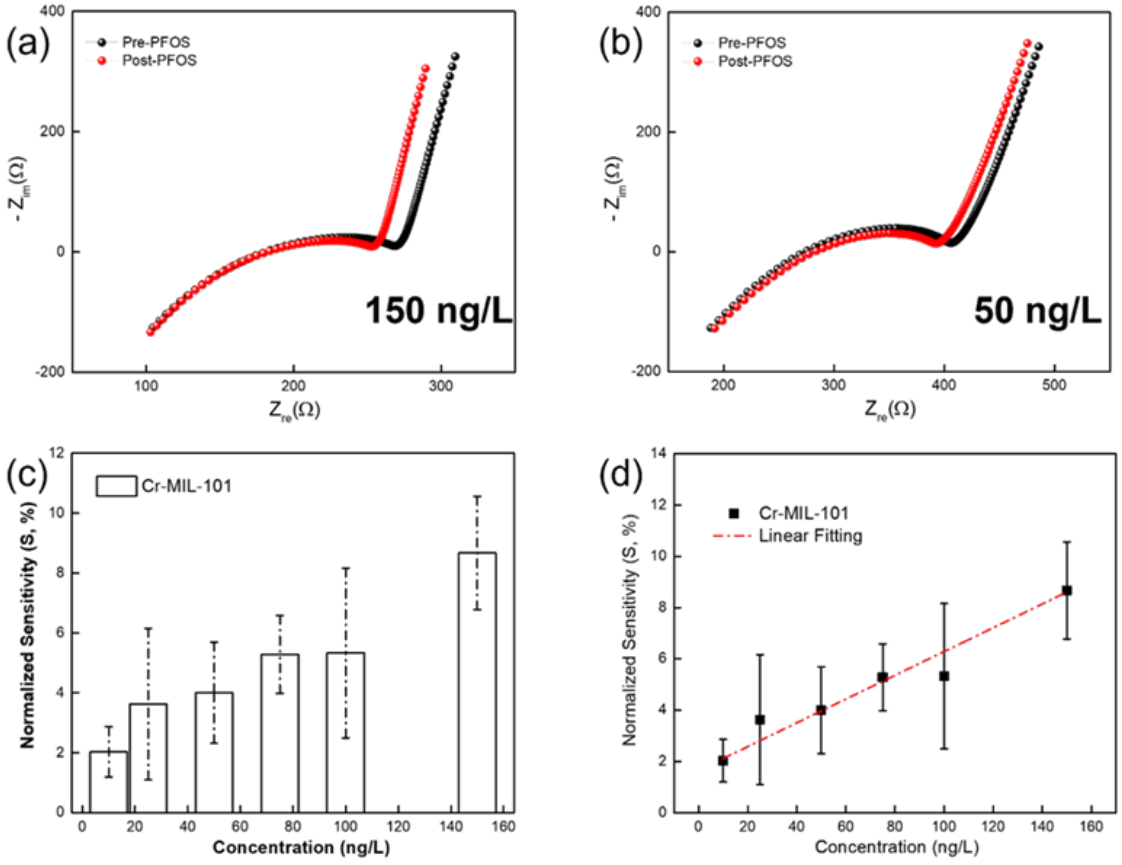

Figure ES-5. Nyquist Plots of the EIS Response to Different PFOS Concentrations in Tap Water Solutions (a) 150 ng/L; (b) 50 ng/L; (c) and (d) Plot between PFOS Concentrations in Tap Water and Normalized Sensitivity (S).

A linear relation between PFOS concentration and normalized sensitivity is observed from 10 to 150 ng/L

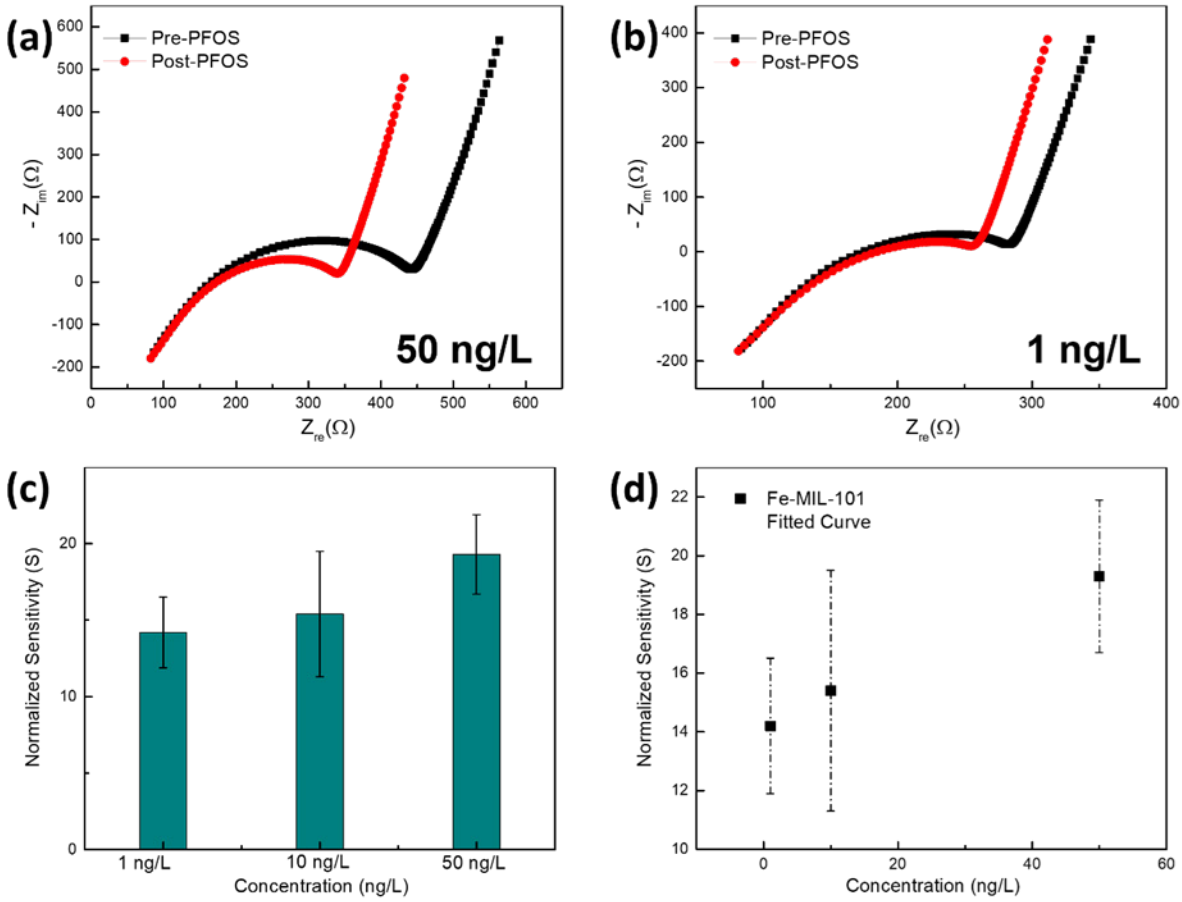

Figure ES-6. Nyquist Plots of EIS Spectra for (a) 50 ng/L and (b) 1 ng/L PFOS. The Black and Red Curve Represents the Nyquist Plot Obtained Before and After PFOS Exposure, Respectively (c) and (d) Plot between PFOS Tap Water Concentrations and Normalized Sensitivity (S) for the Three Concentrations.

PFOA work has been completed using UIO-66 using spiked PFOA samples in phosphate-buffered saline (PBS). PFOA concentrations at 1 µg/L, 500 ng/L, 100 ng/L, 50 ng/L, and 10 ng/L (with four replicates at each concentration) were tested. A data analysis was performed to determine the calibration curve and the LOD. These were then repeated using the MOF UIO-66-NH2. Here, the PFOA spiked 0.1X PBS solutions are passed through the packed channels, and the changes in the EIS signatures were collected and analyzed using an impedance analyzer. Figure ES-7 shows the PFOA detection results based on UIO-66 and UIO-66-NH2. For the UIO-66-based device, five different concentrations were tested, ranging from 1 µg/L to 10 ng/L. However, as shown in Figures ES-7(a) and ES-7(b), we don't see an apparent relationship between the PFOA concentrations and S. The reason is due to the high background blank EIS signals, for blank 0.1X PBS, the device has an S of ~ 14.8%. This can be hypothesized to be caused by the big agglomerated UIO-66 particles which increases the losing probability of UIO-66 from the packed µE pair. Similar trend was observed in the UIO-66-NH2-based device as well. Tests using Cr-MIL-101 based PFAS sensors for PFOA detection showed that these sensors are sensitive to the presence of PFOA as well (Figure ES-8). Hence Cr-MIL-101 based PFAS sensors will lack selectivity between PFOS and PFOA.

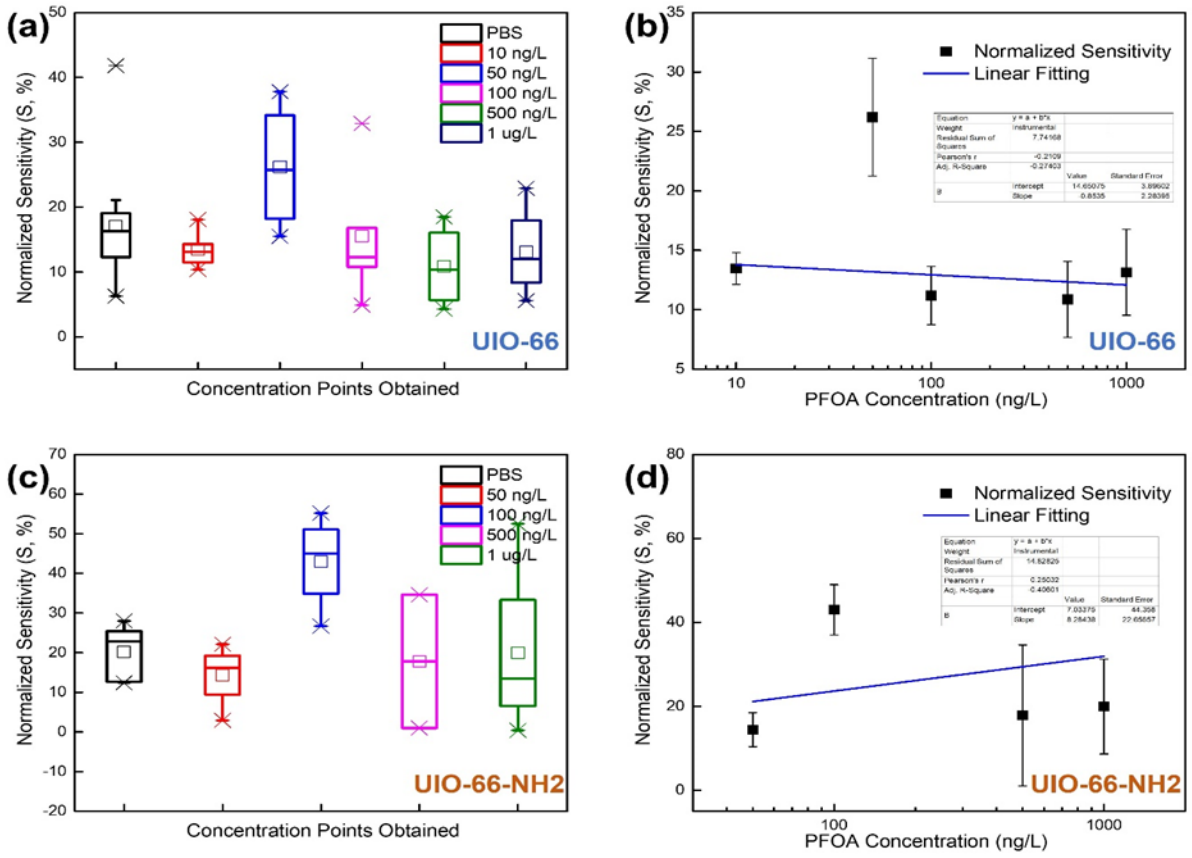

Figure ES-7. (a) Box Plot Statistical Results for Different PFOA Concentrations and Their Corresponding S Based on the UIO-66 Packed NP-μFEC Device. (b) Corresponding Calibration Curve for the Figure (a). (c) Box plot Statistical Results for Different PFOA Concentrations and their Corresponding S Based on the UIO-66-NH2 Packed NP-μFEC Device. (b) Corresponding Calibration Curve for the Figure (c).

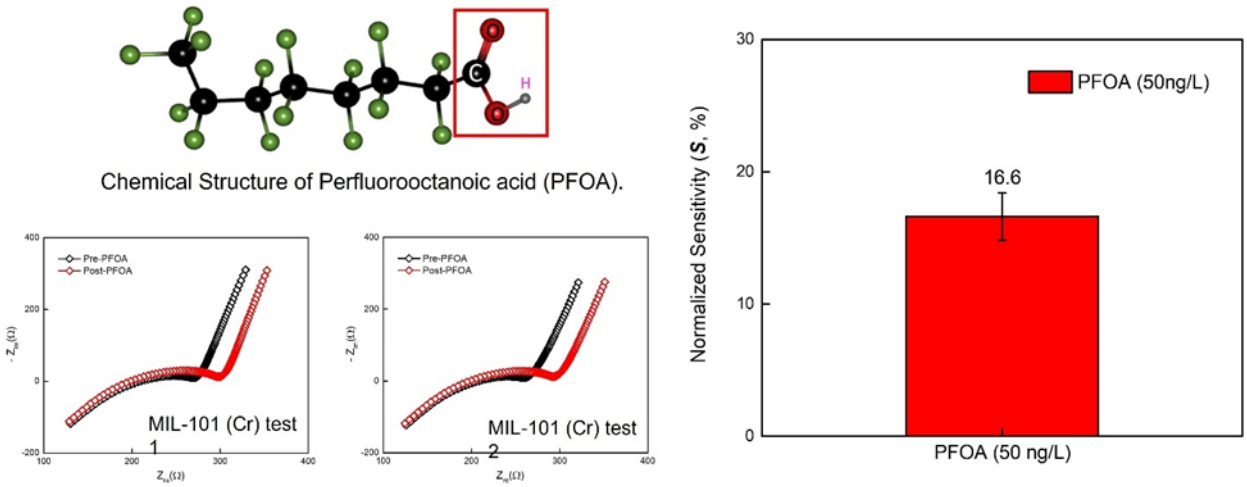

Figure ES-8. PFOA (50ng/L) Testing Results Based on old MIL-101(Cr)

Accuracy, Precision, and Quality Control Assessment

A double-blind accuracy, precision, and quality control (QC) test was performed to assess the precision and accuracy of the current PFAS sensor prototype and was coordinated by Arcadis. The QC test consisted of sending blind PFOS standards in the concentration range of 1 to 150 ng/L along with a DI water blank to NJIT and Pace Analytical lab (Pace). The PFOS standards (15, 47 and 75 ng/L) and the DI water blank were prepared at the Arcadis Treatability Laboratory in Durham, NC. The concentrations were not shared (i.e., prepared as "blind" samples") with either NJIT or Pace. The 47 ng/L PFOS standard was divided into six parts (i.e., identical split samples), with five sent to NJIT and one sent to Pace. Similarly, the 15 ng/L PFOS standard was divided into three parts with two sent to NJIT and one to Pace lab. The 75 ng/L PFOS standard and the DI water blank were divided into two parts each and one part each was sent to NJIT and Pace lab. Hence a total of nine samples were sent to NJIT and four samples were sent to Pace lab. Different concentrations were included to assess accuracy whereas multiple samples of the same concentration were included to check precision. A comparison of the results from this assessment are shown graphically in Figure ES-8. For the assessment, the results from Pace were considered as the actual concentration and the PFAS sensor detections were compared to these results. The results showed that the PFAS sensor results from NJIT ranged from 102 to 580.7 ng/L for the 47 ng/L PFOS standard. This corresponds to 429 to 2420% of the Pace lab result with a standard deviation 56 to 394 ng/L from the Pace result. While precision of the PFAS sensor was at a relative standard deviation (RSD) of 83% from the Pace Lab result. For the 75 ng/L PFOS standard, the PFAS sensor showed a result of 117.3 ng/L which was 267% of the Pace lab result and had a standard deviation of 52 ng/L. Finally, for the DI water blank the PFAS sensor showed a PFOS concentration of 140.7 ng/L while the Pace lab did not detect any PFOS. Based on the results it was concluded that the PFAS sensor would not achieve an accuracy similar to the ELAP accredited lab and a precision ≤30% with the current sensor design, manual packing and heterogeneity of MOFs.nFurthermore, the team has discussed significant error analysis and troubleshooting options and believes that current sensor design cannot come close to achieving any of these criteria. Therefore, a No-Go for the remainder of project activities was recommended. Hence the sensor performance in field samples and the planned field demonstration was not performed.

Addressing Structural Heterogeneity of CR-MIL-101

One of the reasons for high variations in the sensitivity readings at the same target PFAS concentration in due to heterogeneity of particle size in the MOFs used. MOF structural variability or heterogeneity can exist between synthesis batches, where (i) the particle sizes and (ii) pore characteristics (surface area, pore volume) might vary. After observing the lack of precision in PFAS measurements, PNNL characterized the particle size distribution of Cr-MIL-101 MOF and developed a process to achieve uniform particle distribution. The characterization showed that the MOF particles had broadly distributed particle sizes from 0.2- 100 μm (Figure ES-10). The homogenization of particle size involved ball milling the MOF dispersed in ethanol for 48 h followed by centrifugation at high rpm and supernatant separation. The MOF was centrifuged again at low rpm to obtain a uniform particle size distribution as shown in Figure ES-11. This ball-milling procedure, or one like it, will be used to avoid particle size heterogeneity in future experiments.

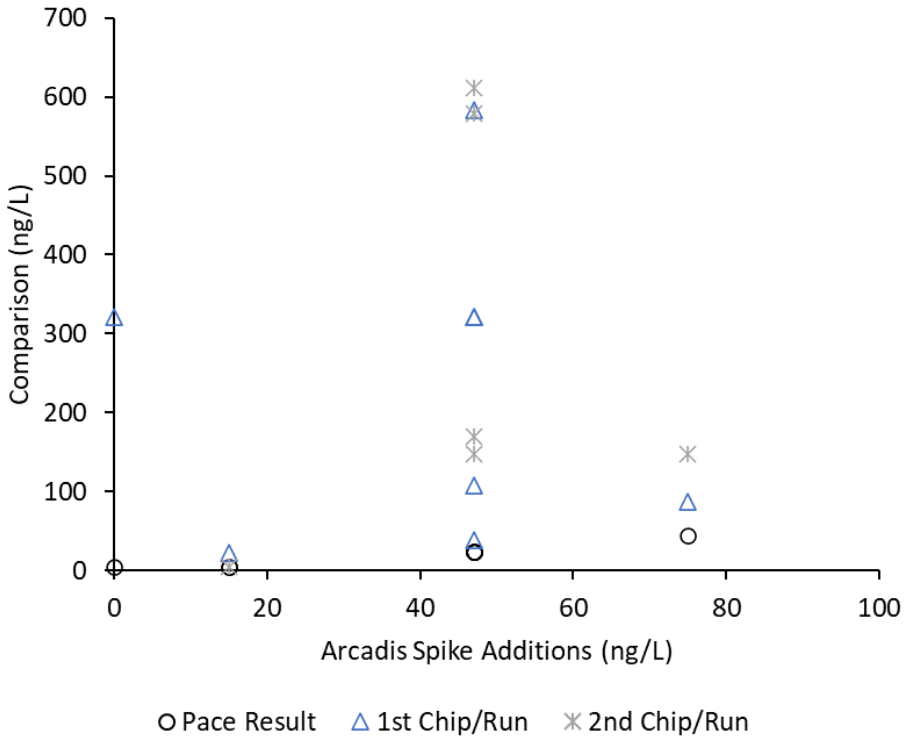

Figure ES-9. A Comparison of the Results from the Accuracy, Precision, and QC Assessment

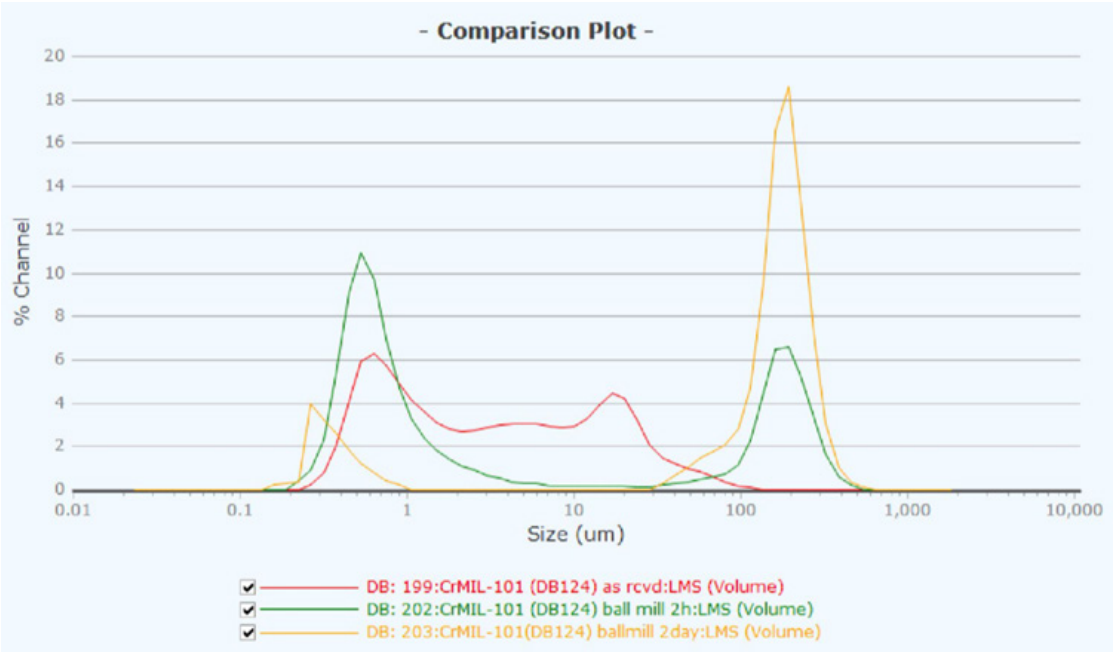

Figure ES-10. Ball Milling of Cr-MIL-101 in an Ethanol Solution, as Received (Red), After 2h (Green) and After 48h (Yellow)

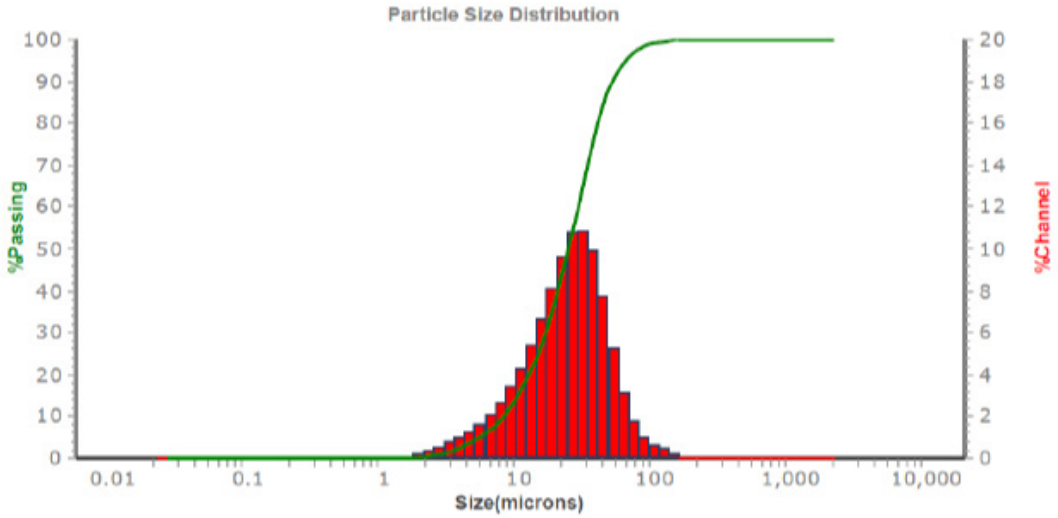

Figure ES-11. Cr-MIL-101, After Ball-milling for 48h in an Ethanol Solution, Followed Centrifuging of the Samples at high RPM first, Followed by Supernatant Separation and Centrifuging Again at Low RPM

IMPLEMENTATION ISSUES

Based on the bench-scale laboratory tests performed, the following implementation challenges and limitations were observed. The Cr-MIL-101 based sensor lacked selectivity between PFOA and PFOS. Additionally, the sensor failed to achieve an accuracy similar to an ELAP-accredited lab and a precision of +/- 30%. The broad particle size distribution was identified as a potential factor for sensor variability. However, the ball milling process developed my PNNL could be used in future to achieve uniform particle size distribution. The current manual packing of MOFs in the sensor is another potential source of variation between sensors. However, to overcome this, a larger chip design with automated packing needs to be adopted. This will likely require complete chip redesign and different chip production equipment which the team currently does not have access to. Moreover, this will require significant additional bench testing and troubleshooting which are beyond the scope of this project. Hence, a No-Go was recommended for the remaining project tasks.

1.0 INTRODUCTION

This Final Report (report) describes the bench scale demonstration and performance assessment associated with Environmental Security Technology Certification Program (ESTCP) Project ER21-5101, which bench-tested the novel PFAS sensor. This report documents the methods, performance data, supporting information for the No-Go decision, recommendation for future research and possible design modifications.

1.1 BACKGROUND

Per- and polyfluoroalkyl substances (PFASs) are a group of anthropogenic chemicals that have demonstrated high persistence due to their physical and chemical properties. Among their many applications, their use in Aqueous Film Forming Foams (AFFF) has resulted in groundwater and soil impacts at DoD sites. Comparatively low regulatory screening levels for PFAS have created a need for fast, reliable, and cost-effective measurement. The PFAS electrochemical sensor is an adaptable technology that will be integrated into a broad range of applications, such as initial characterization and remedy evaluation. This PFAS electrochemical sensor solves many challenges inherent to PFAS impacted site evaluation and remediation efforts: 1) it provides a fast PFAS measurement, which is critical to evaluating performance of a corrective measure, especially when commercial analytical laboratories provide turnaround times of at least 5 business days; 2) it significantly decreases the cost per sample, allowing continuous and more thorough investigation of PFAS impacts with increased statistical significance; 3) it provides selectivity and sensitivity comparable to those obtained by laboratory methods, thereby preventing any data quality concerns.

1.2 OBJECTIVE OF THE DEMONSTRATION

The purpose and scope of ER21-5101 is to field-validate a novel real-time PFAS sensor for use at downstream of PFAS treatment systems at DoD sites to measure PFAS concentrations with high selectivity and sensitivity. This demonstration encompassed the lab validation of the PFAS sensor using PFAS spiked standards followed by its field-validation in a selected DoD site. This demonstration was given a No-Go decision since the sensor failed to achieve the accuracy and precision goals. This report documents the bench-scale data generated, quality control assessment performed, the decisive factors related to the No-Go decision, key lessons learned and areas for future research.

1.3 PROBLEM STATEMENT AND REGULATORY DRIVERS

The desirable physical and chemical properties of PFASs lead to their use in many applications, including chromium mist suppression and in AFFF, which are widely used to fight Class B fires at DoD sites (Barzen-Hanson et al., 2017, Hu et al., 2016). Unfortunately, the desired recalcitrance, durability, and resistance to degradation that lead to their use in commercial products has resulted in numerous source zones and diffuse presence throughout the environment. The United States Environmental Protection Agency (USEPA) had set the health advisory level (HAL) for perfluorooctane sulfonic acid (PFOS) and perfluorooctanoic acid (PFOA) in drinking water to 70 nanograms per liter (ng/L) (individually or combined), with an associated groundwater screening level of 40 ng/L and the Office of the Secretary of Defense has screening criteria for PFOS/PFOA, and perfluorobutane sulfonic acid [PFBS] of 40 ng/L and 40,000 ng/L, respectively (Defense 2019).

Ongoing usage of PFAS-containing products (e.g., AFFF) has resulted in the presence of PFAS at DoD sites several orders of magnitude higher than these screening criteria. PFAS have shown high persistence in the environment; therefore, although the elimination of such substances directly from its sourced application is necessary, the decrease in accumulated human consumption of PFAS is of primary concern. Because of this, many of the US states have comparatively lower screening criteria (for example Vermont has a maximum contaminant level [MCL] for drinking water of five PFAS summed to 20 ng/L). In 2022, USEPA provided interim health advisories for PFOA at 0.004 ng/L and for PFOS at 0.02 ng/L further lowering the HALs. Additionally, final health advisory levels were announced for GenX and PFBS at 10 ng/L and 2000 ng/L respectively (USEPA 2022). There are several methods proposed for rapid PFAS field-analysis; however, each of them has inherent limited application (e.g., colorimetry, field nuclear magnetic resonance [field NMR], mobile liquid chromatography with tandem mass spectrometry [mobile LC-MS/MS], and organo-fluorine methods) (Chen et al., 2013, Weiss-Errico et al., 2017, Zhang et al., 2019, Berger et al., 2005). Consequently, the accepted method for PFAS quantification remains to be physical sample collection in the field with subsequent laboratory analysis at a fixed-base commercial lab, resulting in a significant delay in obtaining results (Barzen-Hanson et al., 2017). Therefore, a need exists for a reliable way to quantify ultra-low PFAS concentrations in the presence of potential geochemical and co-contaminant interference.

This need has motivated researchers to focus on sensors that exploit specific properties of PFAS in a two-step process: (1) by exploiting specific affinity-based interactions, the PFAS are selectively captured from the sample matrix by adsorbing to the sensor, and (2) a unique, measurable response (such as an electrochemical, spectroscopic, or magnetic signal) is tied to this capture. Common challenges associated with available electrochemical sensors include detection limits (i.e., how much PFAS needs to adsorb before measurement), rate-limiting issues with interpretation of the measurable response, cost, and maintenance issues. This research team has developed an in-situ sensor with the novel combination of microfluidic device fabrication and more sensitive capture, which achieves unprecedented sensitivity benefits. The portable electrochemical sensor proposed here uses a metal-organic framework (MOF) for rapid, sensitive, and selective capture of PFAS to be quantified. MOFs are engineered nanoporous materials where pore and surface properties can be designed for specific functionality. For a sensor application, the MOF enables selective capture of PFAS and the ability to interpret this capture at the molecular level with an electrochemical signal that can be used for quantification. The technique was used for quantification of PFOS with a detection limit of 0.5 ng/L (Cheng et al., 2020). This detection limit is at or below current laboratory analysis.

The proposed electrochemical sensor has been demonstrated in controlled laboratory tests for applicability to PFAS (Barzen-Hanson et al., 2017). The proposed demonstration will validate the sensor performance at the field-scale. Data needed for advancement of the PFAS sensor technology for field application includes (1) field-scale sensor analytical performance versus laboratory-based techniques; (2) sensor analytical performance at a range of DoD site conditions to assess selectivity, sensitivity, geochemical and co-contaminant interference, and robustness; and (3) the demonstration of a field-scale prototype to provide necessary functionality and develop a technology transition approach. This validation of field-scale sensor analytical performance will provide the DoD with a technical basis for larger-scale deployment increasing PFAS data density while decreasing the associated analytical turnaround times and cost.

2.0 TECHNOLOGY

This section provides an overview of the novel PFAS sensor, its working principle, and benefits over other type of sensors. Moreover, the method used to achieve selectivity, sensitivity, precision, accuracy and avoid sample interference are also discussed.

2.1 TECHNOLOGY DESCRIPTION

The microfluidic platform design as well as its integration with the engineered nanoporous materials for detection and quantification of PFAS targets has been developed in collaboration between Pacific Northwest National Laboratory (PNNL) and New Jersey Institute of Technology (NJIT). The research was supported by Laboratory Directed Research and Development funding at PNNL and via National Science Foundation funding at NJIT. The ability of the technology to detect ultra-low PFOS concentrations (0.5 ng/L) was published recently in a peer-reviewed article (Cheng et al., 2020). A US patent was filed for this technology in May 2020 (Chatterjee et al., 2020, Motkuri et al., 2019). Similar studies via a complementary electrochemical approach using redox-active adsorptive probes have also demonstrated an ultra-sensitive detection of PFOA (detection limit 1.3 ng/L). A provisional patent has been filed for this complementary technology in December 2019 (Motkuri et al., 2019).

There are two main limitations associated with commonly used analytical sensors for contaminant detection: 1) Sensitivity – the species of interest (analyte) is too dilute in the analyzed matrix and 2) Selectivity – the analyte is often intermixed with many similar species (Barzen-Hanson et al., 2017, Hu et al., 2016, Chen et al., 2013, Weiss-Errico et al., 2017, Zhang et al., 2019). Sensitivity can be mitigated with additional costly steps, such as the concentration of the analyte and amplification of the measurable signal often through optical or electrical enhancement. Selectivity is generally increased with extensive purification steps that isolate the analyte or with elaborate methods and equipment that probe the sample to enhance the measurable signal significantly, such as Surface Plasmon Resonance (SPR) or Surface Enhanced Raman Spectroscopy (SERS). The new electrochemical sensor, developed collaboratively at PNNL and NJIT, utilizes a new electrochemical sensing shear-enhanced, flow-through, nanoporous and capacitive electrode (ESSENCE) technology based on a nonplanar interdigitated microelectrode (NP-IDμE) array described below. The schematics of PFAS detection are shown in Figure 1 (Cheng et al., 2020). The NP-IDμE device (shown on Figure 2) consists of three layers, a top and bottom IDμE and a middle adsorptive layer. The adsorptive probe can be based on porous MOFs, zeolites, covalent organic frameworks (COFs) or hierarchical porous carbons (HPCs). The focus on these adsorbent probes is based on recent observations by PNNL (Motkuri et al., 2014, Bower et al., 2018, Barpaga et al., 2019a, Zheng et al., 2018, Zheng et al., 2017, Zheng et al., 2020) and elsewhere (Chen et al., 2016, Liu et al., 2015, Sini et al., 2018, Ji et al., 2018) of their superfluorophilicity, which allows the separation of perfluoroalkyl chains from other organics. PNNL and NJIT have previously validated the use of a MOF (such as Cr-MIL-101) associated with Carbon Nanotubes (CNTs) for its performance towards selective capture of PFAS. Initial data suggest that the use of ESSENCE technology will boost both sensitivity and selectivity while mitigating fouling and decrease artifacts in the measurable signal.

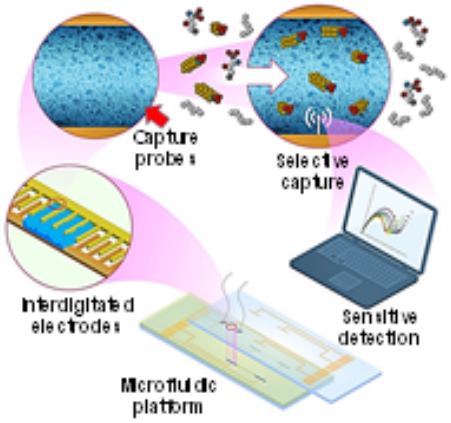

Figure 1. Schematics of PFAS Detection

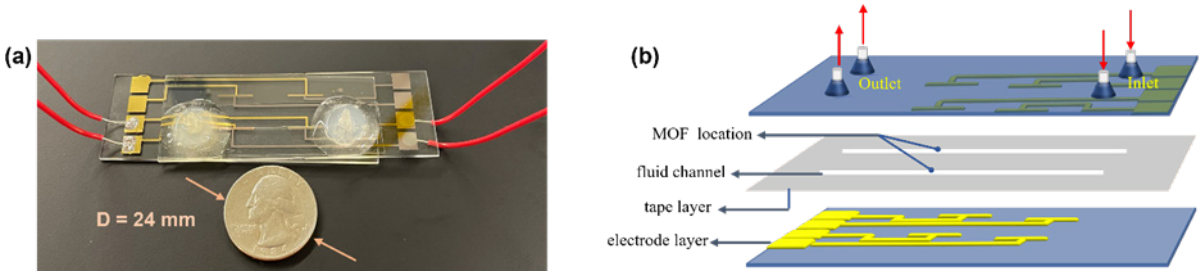

Figure 2. (a) Image Showing MOF-packed NP-µFEC (b) Schematic Diagram if Blank NP-µFEC

The proposed electrochemical sensor has four major benefits over the current generation of electrochemical sensors: (1) the electrode nanoporosity improves selectivity by mitigating non-specific adsorption; (2) the NP-IDµE design fosters nanoconfinment effects, which drastically improves the signal to noise ratio (SNR) and enables the ESSENCE technology to achieve unprecedented sensitivity; (3) the NP-IDµE architecture drastically reduces the distance between the adsorbed analyte and the sensing element, thus overcoming diffusion limitations and assay times while improving the quality of the measurable signal; and (4) finally, since shear force is controllable via flow rate, shear force becomes a customizable design parameter enabling a focused improvement on selectivity.

Electrical Impedance Spectroscopy (EIS) is measured using the array of IDµEs. The EIS spectrum (Nyquist curve) of the MOF (i.e., Cr-MIL-101 or Fe-MIL-101) in a 0.1 molar (M) Phosphate buffered saline (PBS buffer) is a circular region followed by a linear region (Figure 3). The introduction of PFOS in the analyte stream of PBS buffer showed a marked change in the impedance profile of the MOF compared to the buffer solution itself, with a discernible increase in the radius of curvature of the semi-circular region of the Nyquist curves (Figure 3). Upon PFOS capture by the middle MOF layer, the EIS response is modeled using the transmission line equivalent circuit model (commonly used for porous IDµE) shown on Figure 3B using Zview® software (Kaushik et al., 2018, Ding et al., 2017). The charge transfer, or polarization resistance (Rct), is associated with the transfer of the electrons from the electrolyte onto the tightly packed MOF. Rct is heavily dependent on several factors, such as the available surface area of the MOF.

Therefore, the capture of PFOS to the MOF presumably leads to a change in the Rct as a result of decreased available surface area. This is evident from the increased radius of curvature of the semi-circular region of the Nyquist curve.

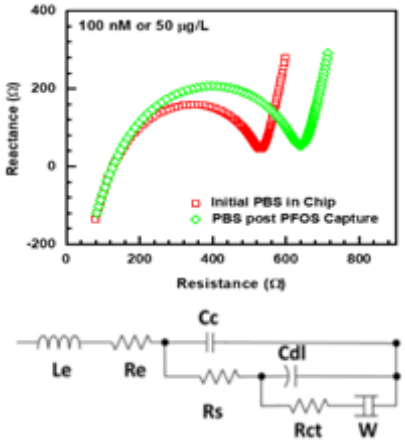

Figure 3. Nyquist Curve from an NP-IDµE Sensor with a Packed Microchannel for PFOS Detection (Above), the Equivalent Circuit for the EIS Response from the NP-IDµE Sensor (Below)

Results from an electrochemical sensor have already been published showing successful demonstration of the proposed PFAS sensor functionality (Gong et al., 2015, Karimian et al., 2018). This preliminary work introduced the conceptual design of our technology – utilizing a microfluidic channel pre-packed with a MOF associated with CNTs known to have high adsorptive affinity for PFOS. Upon passing the analyte through the channel, the selective adsorption of PFOS resulted in clear detection of unprecedently low concentrations. This electrochemical sensing approach has also been used for other water constituents (e.g., pertechnetate [TcO4-] and hardness of water (Chatterjee et al., 2015)). The main selectivity and sensitivity benefits of our design are due to the integration of (1) MOF for PFAS adsorption (Barpaga et al., 2019b) and (2) transmitting a higher quality measureable signal over a shorter distance. Initial data for groundwater testing clearly showed that though both MOFs, Fe-MIL-101 and Cr-MIL-101, are sensitive to the amount of PFOS adsorbed; however, Fe-MIL-101 is more selective for PFOS.

Selectivity

While existing electrochemical sensors for PFAS reported by other groups were limited by adsorptive probes with inadequate selectivity (Chen et al., 2015, Gong et al., 2015, Karimian et al., 2018), we have achieved unique recognition and selectivity of diverse analytes, including PFAS, through strategic adsorptive design. The adsorption is tailored for selective analyte capture by tuning adsorbent topologies, surface functionalities, and pore geometries. The adsorbent probes can be composed of porous MOFs, zeolites, COFs, or HPCs. The focus on MOF adsorbent probes are based on recent observations by PNNL (Motkuri et al., 2014, Bower et al., 2018, Barpaga et al., 2019a, Zheng et al., 2018, Zheng et al., 2017, Zheng et al., 2020) and elsewhere (Chen et al., 2016, Liu et al., 2015, Sini et al., 2018, Ji et al., 2018) of their superfluorophilicity, which allows the separation of perfluoroalkyl chains from other organics. For MOFs and metal-loaded zeolites, the metal centers impart additional selectivity based on their tunable affinity towards PFAS

functional groups enabling differentiation of individual PFAS. The flow-based approach also helps overcome diffusion-based solution resistance, allowing faster measurements (Cheng et al., 2020), and providing another customizable design parameter to further selectivity. Thus, by choosing an appropriate MOF (selective adsorption) and flow rate (customized shear force) combination, we can design a versatile device that is selective for PFAS in water and/or can quantify the total fluorine content of the water. Initial data shows that, for groundwater testing, both Fe-MIL-101 and Cr-MIL-101 are sensitive to the same amount of PFOS, while Fe-MIL-101 is much more selective to PFOS in groundwater.

Sensitivity

The improved detection limit of the PNNL sensor is due to multiple complementary effects. The IDμEs measure approximately 10 microns (μm) in width and 500 μm in length and are therefore microelectrodes with greater SNR than that of macroelectrodes (Cahill et al., 1996, Wightman et al., 2006, Min et al., 2004). Of the multiple advantages of using IDμEs as electrochemical sensors, their high collection efficiencies, rapid detection, ease of fabrication, nanoscale application, and integration with microfluidic chips for multiplexed analytical platforms clearly distinguish IDμEs as best in class for this application (Mecker et al., 2010). By integrating the MOF material (with a high affinity for PFAS) directly into a porous matrix between the IDμE, we've strategically improved the surface area-to-volume ratio and SNR resulting in unprecedented sensitivity and extremely low limits of detection (Cheng et al., 2020, Cheng et al, 2019, Li et al., 2019)). Furthermore, the EIS measurements, which quantify the change in Rct of the MOF as a result of PFAS adsorption, are further enhanced by the non-planar orientation of the IDμE. The NP- IDμE allows complete penetration of the electric field across the MOF adsorptive probe improving signal quality and decreasing the distance of signal transmission. Additionally, NP-IDμE design allows MOFs to have a low electrical conductivity, which in turn provides expanded ability to tune the MOF adsorptive probe for a particular analyte (e.g., PFAS) rather than tune an analyte-specific adsorptive probe for improved electrochemical properties. Increased signal transduction due to the NP-IDμE with MOF materials greatly improves the detection limit. We have recently shown selective PFOS sensing from a multicomponent matrix with a quantification of 0.5 ng/L (Cheng et al., 2020). This matches the detection limits of some high quality laboratory-based PFAS analytical methods. The electrochemical sensor can be expanded to other PFAS by tuning the MOF adsorbent probes.

Sample Interference

Sample interference on PFAS sensor readings may be potentially caused by water quality parameters such as ionic strength, hardness, pH, and co-contaminants such as dissolved organic carbon (DOC) and other PFASs. Ideally, the final PFAS sensor prototype developed through this project will be robust and can be used to detect PFAS concentrations in widely different water matrices. While the budget and scope of this project are not intended to rigorously test all possible ranges for all water matrix parameters, laboratory tests will be completed to assess the general significance of water matrix interferences for critical parameters. This will allow the prediction of water matrix effects on sensor performance for specific applications and may guide site-specific calibration and optimization. Each sensor will be unique and produce accurate results only in the water it is optimized for. In this project, the sensor will be ultimately optimized and calibrated for the specific water matrix representative of the anticipated field test at Willow Grove.

The sensor will assess PFAS trends and breakthroughs in the treatment system. In similar applications, temporal variations in water quality parameters like pH, ionic strength, and DOC are not expected; therefore, sensor performance and precision remain stable. Nevertheless, we planned to investigate the effect of individual parameters on PFAS sensor recovery and build standard curves based on the PFAS sensor response at the same PFAS concentration but varying-parameter concentration. The study will look into the effect of DOC, pH, ionic strength, hardness, and the presence of other PFASs on PFAS sensor recovery. A detailed description of each factor and the testing plan are provided below.

DOC

DOC could lower PFAS recovery by competing for sorption sites, altering the surface charge of the sorbent, thereby repelling anionic PFASs, blocking entryway to sorption sites, complexation with PFASs, and heavier DOC replacing adsorbed PFASs. Since the primary suggested use of this sensor is to test for PFAS breakthroughs from water treatment plants designed to remove PFAS from water using sorbents such as GAC and ion exchange resin, a significant amount of DOC is not expected in the effluent water. Hence DOC is not expected to have much interference in the sensor readings in this application. Nevertheless, tests at different DOC concentrations will be carried out to understand the effect of DOC on PFAS sensor readings.

The typical groundwater DOC range ranges from 0-5 mg/L. To study DOC's effect on PFAS readings, humic acid will be spiked to achieve different DOC concentrations. The solutions will be prepared at humic acid concentrations of 0, 0.5, 1, 2, and 5 mg/L and PFAS concentrations of 1 and 100 ng/L. Tests will be conducted for all six PFASs included in this study. The results will create standard curves for each PFAS with PFAS sensor readings at each DOC concentration.

pH

The pKa values of the six PFAS, PFOA, PFOS, PFHxA, PFHxS, PFBA and PFBS range from -3.31 to +3.8. Hence at environmentally relevant pH, these PFASs are in their anionic form and can be repelled by the negative charge on the sorbent surface, causing a lower recovery. Since the surface charge on the sorbent surface can be influenced by the pH, this can also affect the PFAS recovery. A pH lower than the point of zero charge makes the sorbent positively charged, thereby improving PFAS recovery, whereas a higher pH could lower PFAS recovery. The variation in PFAS recovery with pH is not linear and is more pronounced in the pH range close to the point of zero charges. Typical groundwater pH ranges from 6 to 8.5; however, to cover a more comprehensive pH range, the study will include pH from 5 to 9. A standard curve with different pH values and their corresponding PFAS reading from the sensor will be plotted.

Solutions of different pH will be prepared by spiking either HCl or NaHCO3. Solutions will be spiked with a single PFAS at a particular concentration, and the corresponding sensor readings will be recorded. Tests will be conducted for all six PFASs, at pH of 5, 6, 7, 8, and 9 and PFAS concentrations of 1 and 100 ng/L.

Ionic strength

High ionic strength and the presence of specific ions at relatively high concentrations could affect the sorption and solubility of some PFASs. Cations could neutralize the negative charge on the

sorbent, thereby reducing the repulsion between the sorbent surface and anionic PFASs. Typical ionic strength observed in groundwater range from 0.001M to 0.02M. Since sodium chloride is the most common salt present in groundwater, a study on the effect of ionic strength on PFAS sensor reading will be conducted using PFAS spiked sodium chloride solutions. Sodium chloride concentration representing ionic strength ranging from 0.001M to 0.02M will be tested against the same PFAS concentration to assess the variation in the sensor signal.

For sodium chloride, since ion strength is equal to the concentration, the tests will be carried out six different NaCl concentrations of 0, 0.001, 0.002, 0.005, 0.01, and 0.02M. Standard curves for all six PFASs considered for this study will be created at two different PFAS concentrations of 1 and 100 ng/L.

Hardness

Hardness is caused by the presence of calcium and magnesium ions. Being divalent, Ca^{2+} and Mg^{2+} could potentially improve PFAS recovery through the bridging effect. In the United States, the typical range of hardness in groundwater range from 0 to 250 mg/L as $CaCO_3$.

To test the effect of hardness on PFAS sensor readings, solutions of varying hardness will be prepared by adding $CaCl_2$ to achieve the target hardness, followed by spiking equal amounts of PFAS. Tests will be carried out at hardness 0, 50, 100, 200, and 250 mg/L as $CaCO_3$. These hardness values correspond to $CaCl_2$ concentrations of 0, 56, 111, 222, and 278 mg/L respectively.

Other PFASs

The sensor will be optimized to quantify six PFASs: PFOA, PFOS, PFHxA, PFHxS, PFBA, and PFBS. The sensor recovery of a particular PFAS can be adversely affected by other PFASs. This is especially significant for short-chain PFASs such as PFBA, which could be desorbed and replaced by more hydrophobic, longer-chain PFASs from the sorbent surface. The other challenge is to quantify multiple PFASs simultaneously in a solution containing different PFASs.

To study the effect of other PFASs on the sensor recovery of a particular PFAS, individual PFASs will be tested against PFAS mixture solutions. As there are more than 5000 different PFASs, testing their effect on the sensor recovery of the six PFASs included in this study is not feasible. Instead, this study will explore the recovery of individual PFASs in the presence of the other five PFASs included in this study. The six PFASs considered in this study are representative of short, medium, and long-chain PFASs.

Since the proposed point of use of the PFAS sensor is in the downstream effluents of lead and lag reactors and its intended use is to check for a breakthrough, PFAS concentrations exceeding 100 ng/L are not expected. Using this information, the effect of co-occurring PFASs will be studied in deionized water solutions spiked with the target PFAS and a mixture of the remaining five PFASs. The PFAS mixture will have individual PFAS concentrations at 1, 10, 20, 50, and 100 ng/L, whereas the targeted PFAS concentration will be tested at 100 ng/L. A standard curve for each PFAS will be created with the sensor response for the target PFAS at PFAS mixture concentrations of 1, 10, 20, 50, and 100 ng/L.

To address the second challenge, measuring the concentration of different PFASs simultaneously, multiple sensors will be arranged in series or parallel configurations, with each sensor optimized for a particular PFAS. An example is shown in Figure 4. PFOS will be taken up preferentially in line 1 slot 1, PFOA in line 2 slot 1, PFBS in line 3 slot 1, and PFBA in line 4 slot 1. The EIS signal from slot 1 in each line will be primarily from PFOS, PFOA, PFBS, and PFBA (initial concentration estimate using already generated calibration curves). Some adsorption of the other quantities will also occur; hence, the values obtained need to be corrected. This correction will be done using the EIS readings from the following 3 slots in each line and writing an algorithm to correct it. There is redundancy in the calculations by having 4 lines and 4 slots, 16 total. This algorithm is expected to be further refined for multiple sensors in parallel or series to discriminate across different PFAS molecules selectively.

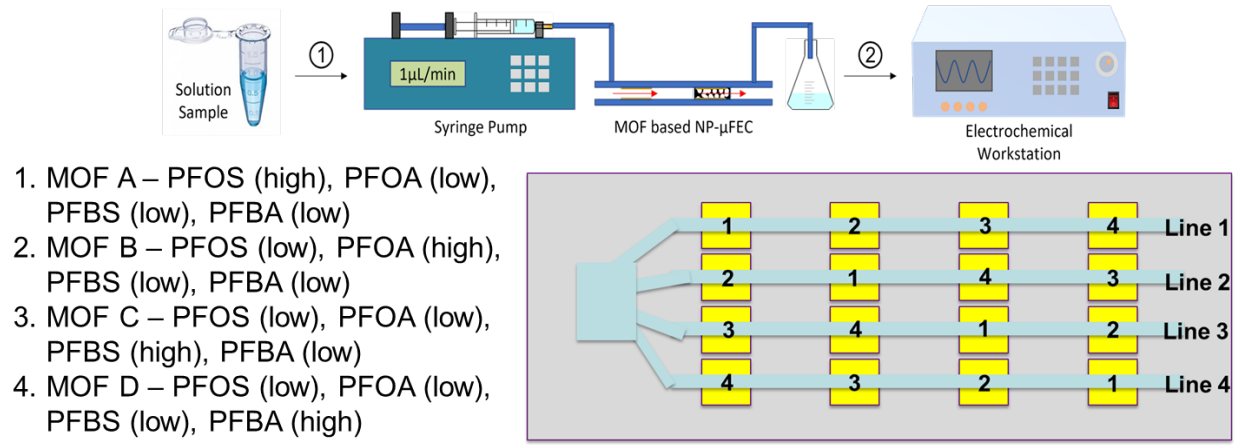

Figure 4. The Figure Above Shows a Chip with Multiple Sensor Chips in Series and Parallel.

Chip 1 has MOF A, Chip 2 has MOF B, Chip 3 has MOF C and Chip 4 has MOF D. For each MOF, the sensitivity and selectivity to different PFOS molecules are shown on the left with high means high sensitivity while low means low sensitivity

Reproducibility and Precision

As discussed earlier, each sensor will be optimized to work in a particular water matrix for a particular PFAS. As long as the water quality parameters, DOC, and other PFAS concentrations remain relatively stable, the sensor can provide reproducible results.

Performance objective: The sensor reading in real-world water matrices will be compared to results from the ELAP-certified lab for reproducibility and precision. The objective will be to achieve a standard deviation less than or equal to the standard deviation achieved by the ELAP-certified lab. For this task, an effluent sample from the Willow Grove treatment plant will be spiked with the six PFASs considered for this study at a concentration of 100 ng/L each. From this sample, five aliquots will be taken, each divided into two, with one half used for PFAS sensor detection and the other sent to an ELAP-certified lab. The precision of the PFAS sensor was then compared to the lab's based on the standard deviation of their readings. This task will also be repeated at a PFAS concentration of 1 ng/L.

Measurement accuracy

The intended use of the sensor is to detect PFAS breakthroughs in the effluent of treatment plants. In such a scenario, considerable variations in water quality parameters and co-contaminant concentrations are not expected. Since each sensor will be unique and optimized to work in a particular water matrix, the sensor can provide accurate results as long as there are no significant variations in water quality parameters and co-contaminant concentrations. Nevertheless, more than 20% variation in the PFAS sensor reading is not expected for the entire concentration range influencing water quality parameters and co-contaminants.

Performance objective: The objective will be to achieve less than 20% difference in sensor readings for the range of variation expected for water quality parameters such as pH, ionic strength, hardness, and co-contaminants such as DOC and other PFASs. For this study, synthetic samples spiked with a target PFAS and one influencing parameter or co-contaminant will be studied to ensure the variation in PFAS sensor reading doesn't vary more than 20% during the entire concentration range of the corresponding water quality parameter or co-contaminant. The range of concentrations of water quality parameters such as pH, ionic strength, hardness, and co-contaminants such as DOC and PFASs to be tested are given in the sample interference section. The accuracy of the sensor reading will be tested at target PFAS concentrations of 1 and 100 ng/L.

Relative response factors

The standard curves developed to study sample interference from water quality parameters, and co-contaminants will be utilized to predict the correct PFAS concentration based on the concentration of the corresponding water quality parameter or co-contaminant. This will be achieved by using the equation of the trendline that matches the standard curve the best. Based on the PFAS sensor response peak, the measured concentration of the influencing parameter, and the equation of the standard curve for that particular parameter, the sensor could arrive at the correct PFAS concentration in the water matrix.

3.0 PERFORMANCE OBJECTIVES

The project objectives are the field demonstration of the electrochemical sensor for rapid and selective quantification of PFAS and an evaluation of the electrochemical sensor's performance (i.e., accuracy, precision, sensitivity) on samples collected from DoD sites. The performance objectives are given in Table 1. The following specific technical objectives will be used to guide activities:

- Quantify PFAS sensor performance (i.e., accuracy, precision, sensitivity) with comparison to laboratory-based analysis of relevant PFAS standards and calibrate sensors for performance. The comparison will be made by submitting split samples to an Environmental Laboratory Accreditation Program (ELAP)-accredited laboratory for analysis by LC-MS/MS.
  - Go/no-go decision based on sensor performance versus the laboratory standards. We are targeting agreement between our sensor and the laboratory-based analysis of within 30%.
- Quantify PFAS sensor performance (i.e., accuracy, precision, sensitivity) with comparison to laboratory-based analysis of representative field samples. The comparison will be made by submitting split samples ($n \geq 3$ for each sample tested) to an ELAP-accredited laboratory for analysis by either PFAS by LC-MS/MS (according to Table B-15 of DoD QSM 5.3 [or latest version]) or by EPA method 533.
  - Go/no-go decision based on sensor performance versus the laboratory samples. We are targeting agreement between our sensor and the laboratory-based analysis of within 30%.
- Identify sensor configuration adjustments for field application and any limitations for use with field samples (e.g., geochemical or co-contaminant interferences).
- Demonstrate a field-deployable sensor configuration for a PFAS water treatment and/or monitoring application. PFAS sensor performance will be evaluated onsite by comparison of sensor measurements with laboratory-based analysis. The comparison will be made by submitting split samples ($n \geq 3$ for each sample tested) to an ELAP-accredited laboratory for analysis by either PFAS by LC-MS/MS (with DoD QSM 5.3 [or latest version] compliance) or by EPA method 533. Technology transfer will be initiated following successful completion of field demonstration.

Table 1. Performance Objectives

Performance Objective	Data Requirements	Success Criteria
Quantitative Performance Objectives		
Evaluate the comparability of data from the electrochemical sensor to traditional laboratory-based analytical techniques for PFAS in clean water samples	Results of split samples from laboratory generated PFAS solutions analyzed with our sensor and at an ELAP-accredited laboratory for PFAS consistent with DoD QSM 5.3 (or latest version)	• Accuracy – Equivalent to an accredited laboratory • Precision - %RSD of no more than 30% Performance variation- Less than 20% difference for a range of water matrices
Evaluate electrochemical sensor configuration/material combinations	Results from multiple MOF adsorptive probes tested in an electrochemical sensor with laboratory generated PFAS solutions	The MOF adsorptive probe with the lowest detection limit will be accepted. The accepted probe must have a % RSD of no more than 30% and a detection limit- at or below EPA screening level of 40 ng/L
Evaluate the comparability of data from the electrochemical sensor and traditional laboratory-based analytical techniques for field samples (PFAS contaminated water from DoD)	Results of split samples ($n \geq 3$) from samples collected from DoD field sites analyzed with our sensor and at an ELAP-accredited laboratory for PFAS consistent with DoD QSM 5.3 (or latest version)	• Accuracy - within 30% of accredited laboratory • Precision - %RSD of no more than 30% Sensitivity - at or below USEPA screening level of 40 ng/L
Evaluate impact of site conditions, geochemistry, as well as the need for sample pre-treatment	Results from field samples collected from at least 3 different DoD sites with varied local geochemistry	Preparation for analysis in the field takes less than 30 minutes
Evaluate sensor configuration at a water treatment application	Results of split samples ($n \geq 3$) from samples collected from the water treatment system with our sensor and at an ELAP-accredited laboratory for PFAS consistent with DoD QSM 5.3 (or latest version)	• Accuracy - within 30% of accredited laboratory • Precision - %RSD of no more than 30% • Sensitivity - at or below USEPA screening level of 40 ng/L • Regenerability or some mechanism for continuous/regular periodic use
Qualitative Performance Objectives		
Field operational experience	Interviews with field staff	• Robustness • Response time Ability to integrate with treatment system

4.0 SITE DESCRIPTION

In preparation for a potential field testing, the team conducted a preliminary site visit to Willow Grove Naval Air Station in August 2022 and reviewed the on-site treatment system. Based on this site visit, the team determined this would be an excellent candidate site for field testing an eventual sensor. However, because a "No-Go" was recommended, no further field testing was conducted.

5.0 PERFORMANCE ASSESSMENT

5.1 SELECTION OF MOFS BASED ON PFAS SORPTIVE CAPACITY

5.1.1 PFOS

Prior to the sensor testing of PFOS detections, a comparison of PFOS capture on four MIL-type materials, Cr-MIL 101, Fe-MIL-101, Fe-MIL-100, and Fe-MIL-88b, at levels near and below EPA health advisory levels (parts per trillion, ppt) as well as at levels as high as 10 mM (parts per million, ppm) were conducted to study the uptake capacity of these MOFs. Sorption at low concentrations were confirmed using LC-MS/MS whereas sorption at ppm levels used NMR spectroscopy (Fig. 5). Both Fe-MIL-100 and Fe-MIL-101 showed high sorption capacities, while Cr-MIL-101 showed saturation. The sorption experiments will be repeated with increased concentrations to achieve saturation capacities. The chosen easy-to-make, inexpensive materials from the MIL family, paired with its facile, easily scalable synthesis procedure that yields reproducibility and high-quality material, are characteristics that make it especially desirable for field deployment.

5.1.2 PFOA

Prior to the sensor testing for PFOA detections, a sorption study was conducted using UiO based MOFs. These MOFs showed have shown favorable conditions for the PFOA capture in water is the zirconium-based UiO-type framework. Synthesis procedures of these types of MOFs usually involve using acids, sometimes in an aqueous solution, that trigger the formation of octahedral $Zr_6O_4(OH)_4$ nodes linked by principally aromatic, linear dicarboxylate. These linkages show excellent stability against hydrolysis under neutral and acidic conditions accompanied by PFAS solutions. A series of zirconium-based UiO-66-based MOFs, such as UiO-66, UiO-66-NH_2, UiO-66-$(OH)_2$, UiO-66-$(COOH)_2$, and UiO-66-F4 were synthesized and characterized by XRD and N_2 physisorption measurements. The fully characterized materials were tested for PFOA capture at ppm levels, and the preliminary results are shown in Figure 6. The UiO-66 and its F4 substituted material showed high sorption capacities. More detailed analysis, stability testing of the materials, and repeated capture capabilities of the PFOA materials are in progress.

5.1.3 Perfluorobutanoic acid (PFBA)/ Perfluorobutanesulfonic acid (PFBS)

By considering the sieving effect and physical adsorption, an attempt was made to test the capture capability of the low-pore MOFs for both PFBA and PFBS in water at ppm level concentrations. Preliminary results showed positive results and are discussed below.

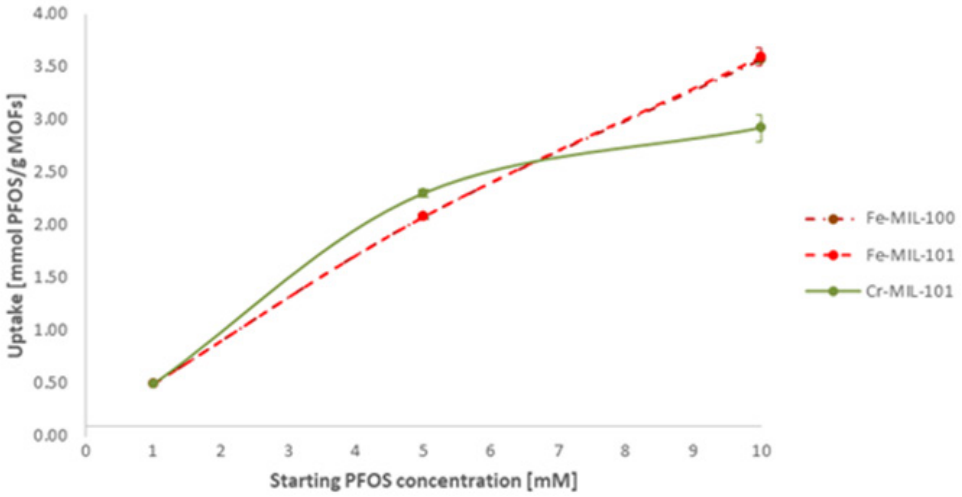

Figure 5. PFOS Capture at ppm Levels in MIL Family of MOFs

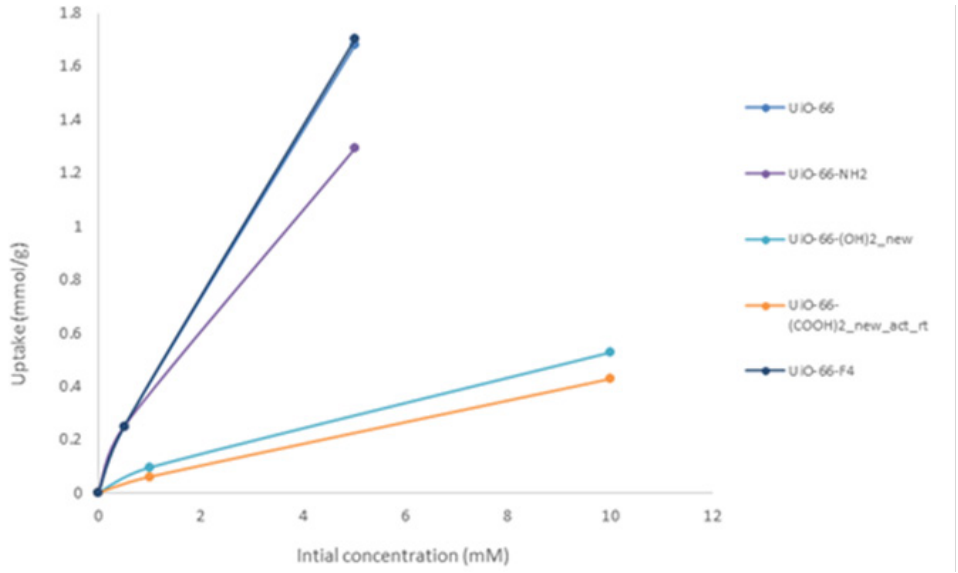

Figure 6. PFOA Capture at ppm Levels in the UiO-66 Family of MOFs

5.2 SENSOR PERFORMANCE WITH LABORATORY STANDARDS

PFAS sensor performance (i.e., accuracy, precision, sensitivity) was assessed and optimized in PFAS standards and calibration curves were generated based on the sensor's sensitivity at different concentrations. The task was designed to include testing the sensor performance in tap water solutions spiked with individual PFASs. The six PFASs targeted in this study are PFOS, PFOA, PFHxA, PFHxS, PFBA and PFBS. Each PFAS compound was intended to be tested individually for concentrations ranging from 10 to 150 ng/L and the sensor's normalized sensitivity to different PFAS concentrations will be developed. Each reading uses a new sensor, hence each point in the calibration curve requires a separate sensor. Additionally, Nyquist plots of electrochemical impedance spectroscopy (EIS) spectra to different PFOS concentrations were created to compare two MOF materials, Cr-MIL-101 and Fe-MIL-101.

In parallel, a comparison of different MOFs, namely, Fe-MIL-100, Fe-MIL-101, Cr-MIL-101, and various MOFs of the UiO-66 family were conducted to test their sorption capacity for PFOS, PFOA, PFBS and PFBA.

5.2.1 Detection of Perfluorooctanesulfonic acid (PFOS) in spiked tap water solutions

Detection of PFOS in tap water solutions was demonstrated using NP-μFEC. Cr-MIL-101 and Fe-MIL-101 have been used as transducer materials for the sensor to evaluate their characteristic as potential materials for selectivity and sensitivity. Six different PFOS concentrations (10, 25, 50, 75, 100, and 150 ng/L) have been tested, and relevant results are presented in Figure 2. Cr-MIL-101 for PFOS tap water analysis is completed. For the analysis, the EIS data from 1.2 kHz to 100 MHz was fitted using the Randall equivalent circuit and using EIS software Zsigmawin (Cheng et al., 2020).

As can be seen from Fig. 7 and Fig. 11, Fe-Mil-101 shows higher sensitivity for PFOS than Cr-Mil-101. The SEM characterization of Cr-MIL-101 after PFOS detection is given in Figure 8(a). The EDS layered image of S and F elements is shown in Figure 8(b). Figures 8(c) and (d) show the clear existence of these two elements. A content table of different possible elements within the scan area is attached in Figure 8(e).

Figure 9 illustrates SEM images of Fe-MIL-101 and Fe-MIL-101-based NP-IDμE devices before and after PFOS capture. EDX images showing the distribution of different elements within the Fe-MIL-101 framework after PFOS exposure are provided in Figure 10.

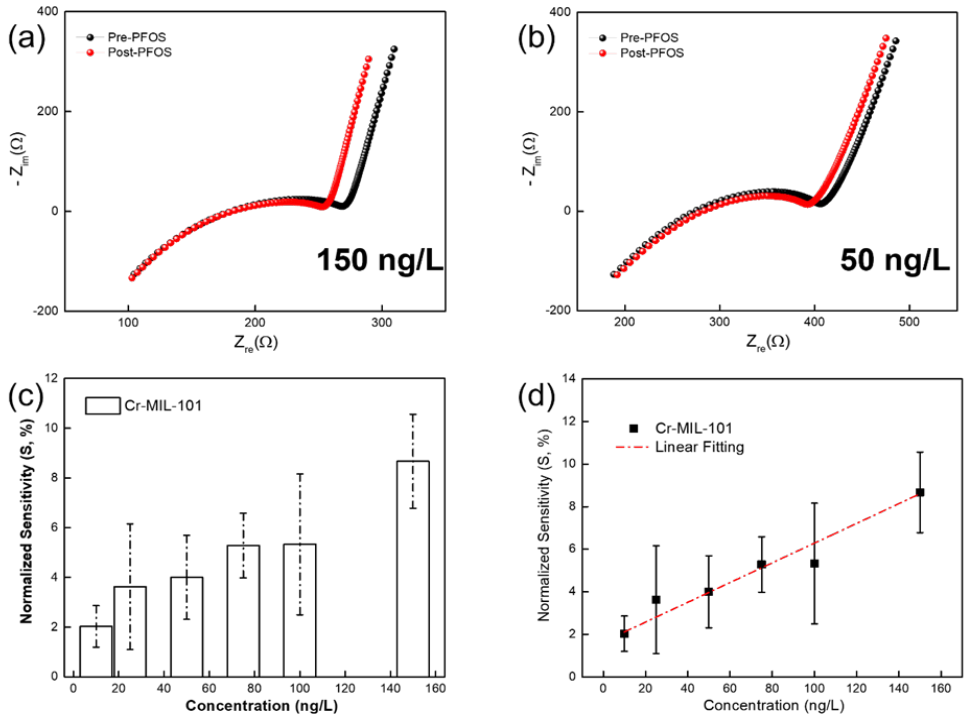

Figure 7. Nyquist Plots of the EIS Response to Different PFOS Concentrations in Tap Water Solutions (a) 150 ng/L; (b) 50 ng/L; (c) and (d) Plot between PFOS Concentrations in Tap Water and Normalized Sensitivity (S).

A linear relation between PFOS concentration and normalized sensitivity is observed from 10 to 150 ng/L

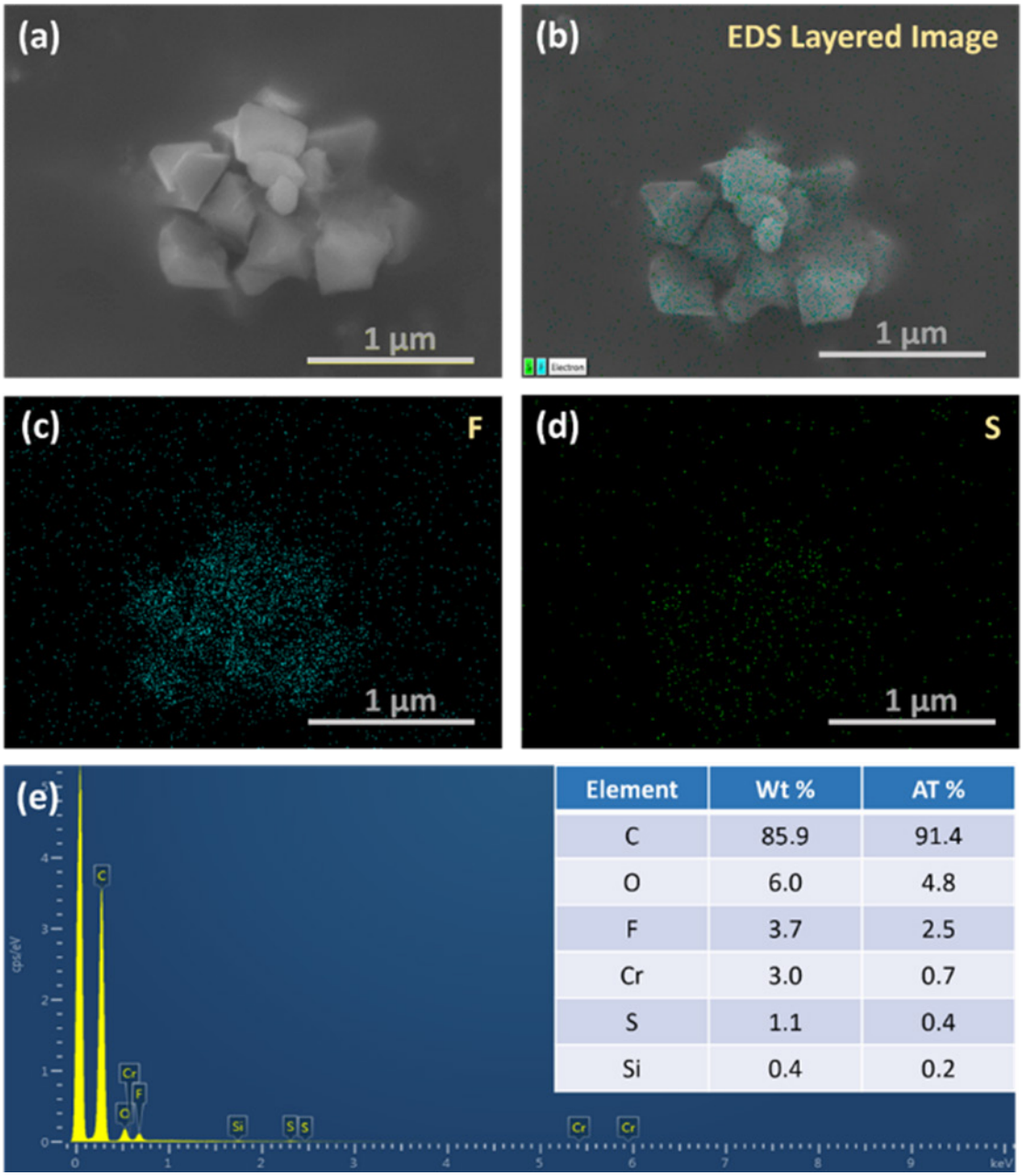

Element	Wt %	AT %
C	85.9	91.4
O	6.0	4.8
F	3.7	2.5
Cr	3.0	0.7
S	1.1	0.4
Si	0.4	0.2

Figure 8. a) SEM Image of a Cluster of Cr-MIL-101 (post-PFOS). (b) Element of S and F's EDS Layered Image. (c) and (d) Is the Element Distribution Image of S and F, Respectively. (e) The Content Statistics of the Different Possible Elements in the Scan Range.

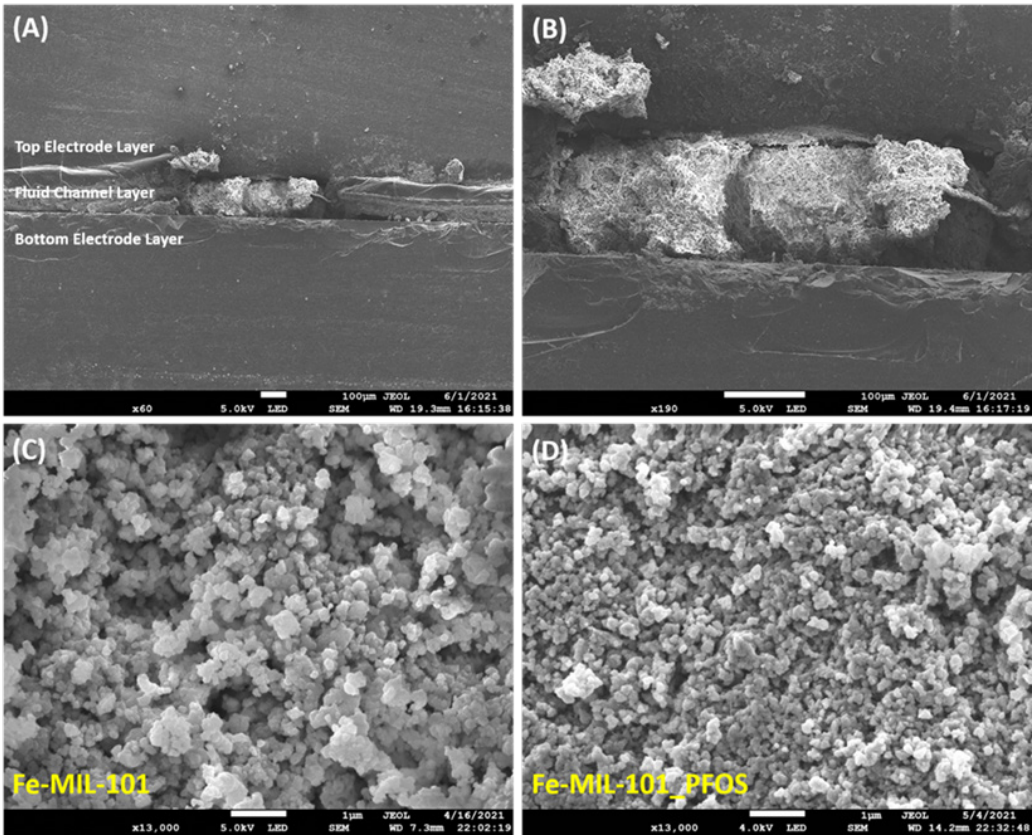

Figure 9. Cross-section SEM Images of Fe-MIL-101-based NP-IDμE Device (A and B). SEM Images of Fe-MIL-101 Before (C) and After (D) Exposure to PFOS.

The scale bar is 1μm.

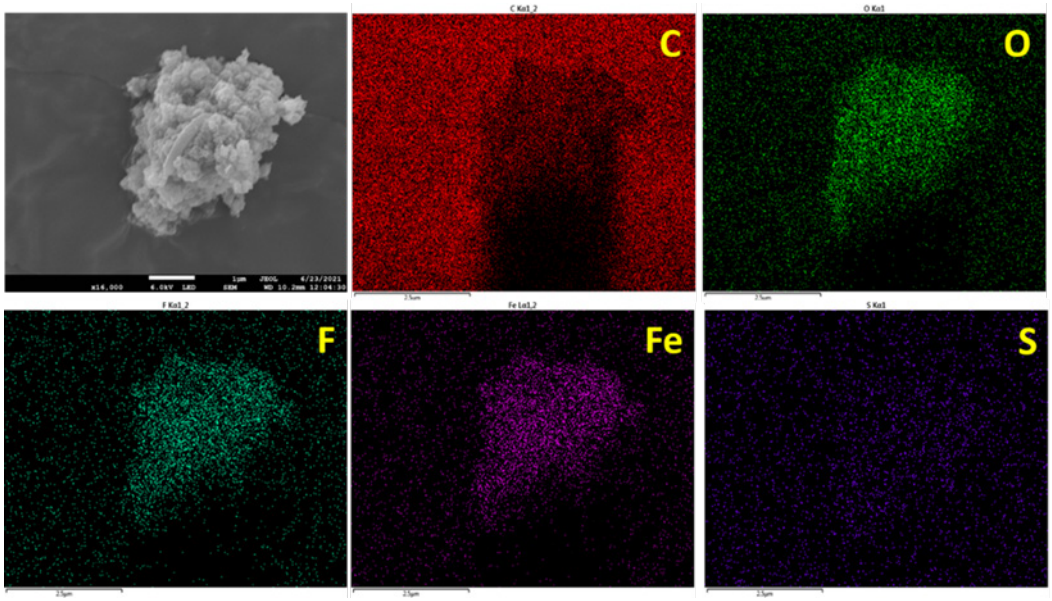

Figure 10. EDX Images of Different Element Distribution within the Fe-MIL-101 Framework after PFOS Exposure

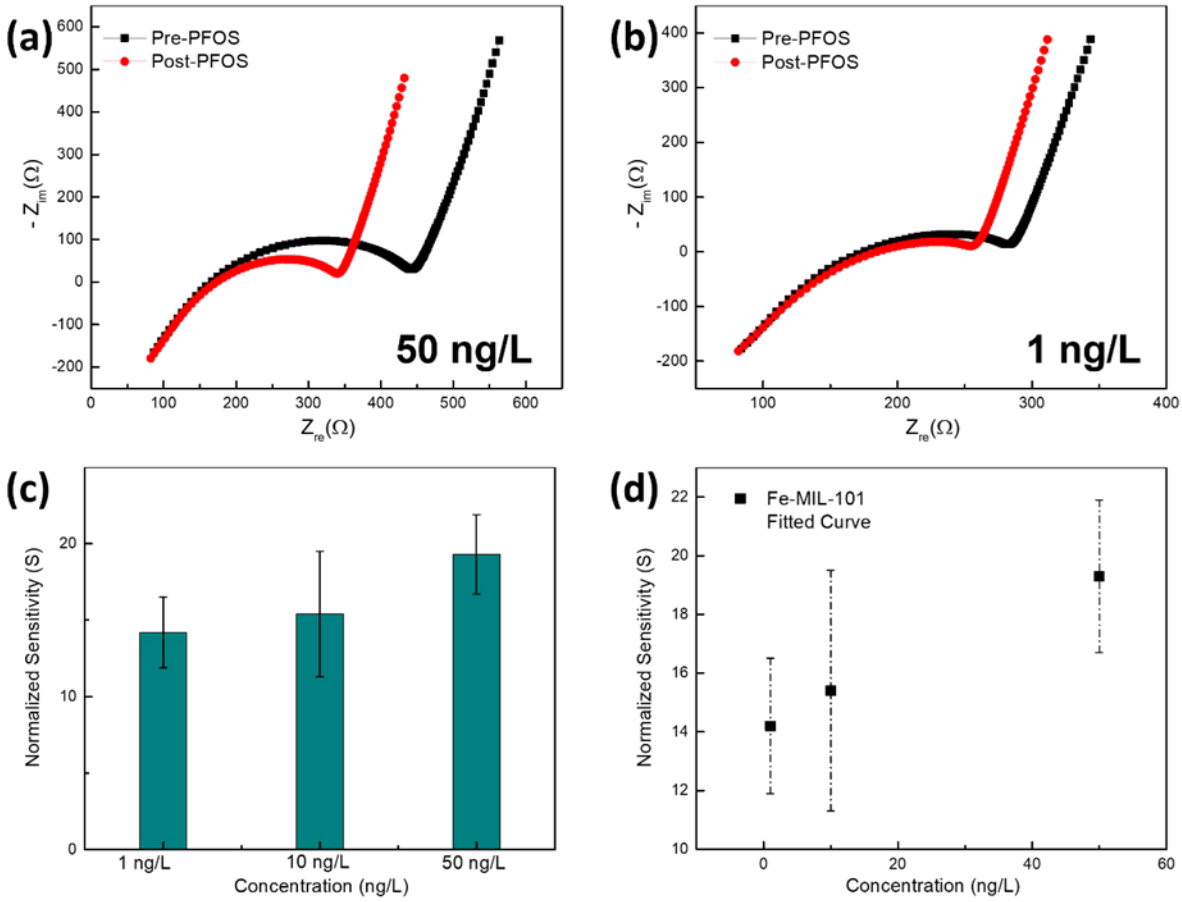

Figure 11. Nyquist Plots of EIS Spectra for (a) 50 ng/L and (b) 1 ng/L PFOS. The Black and Red Curve Represents the Nyquist Plot Obtained Before and After PFOS Exposure, Respectively (c) and (d) Plot Between PFOS Tap Water Concentrations and Normalized Sensitivity (S) for the Three Concentrations.

5.2.2 Detection of PFOA in spiked tap water solutions

PFOA work has been completed using UIO-66 using spiked PFOA samples in phosphate-buffered saline (PBS). PFOA concentrations at 1 µg/L, 500 ng/L, 100 ng/L, 50 ng/L, and 10 ng/L (with four replicates at each concentration) were tested. A data analysis was performed to determine the calibration curve and the LOD. These were then repeated using the MOF UIO-66-NH2. Post PBS, spiked water samples in tap water were planned to be run to see if the calibration curve changes in tap water in contrast to PBS. However, since a No-Go was recommended, these tests were not conducted.

The two MOFs tested and the corresponding optical images of their packed channel in given in Fig. 12. Here, the PFOA spiked 0.1X PBS solutions are passed through the packed channels, and the changes in the EIS signatures were collected and analyzed using an impedance analyzer. It should be noted that agglomerated UIO-66 or UIO-66-NH2 “particles” are difficult to mill down to smaller particles, even after quite a long sonication process. This results in the packed channels having relatively high porosity which tremendously affected the results.

Figure 13 shows the PFOA detection results based on UIO-66 and UIO-66-NH2. For the UIO-66-based device, five different concentrations were tested, ranging from 1 µg/L to 10 ng/L. However, as shown in Figures 13(a) and 13(b), we don't see an apparent relationship between the PFOA concentrations and S. The reason is due to the high background blank EIS signals, for blank 0.1X PBS, the device has an S of ~ 14.8%. This can be hypothesized to be caused by the big agglomerated UIO-66 particles which increases the losing probability of UIO-66 from the packed µE pair. Similar trend was observed in the UIO-66-NH2-based device as well. But we can see the tendency, that is, with the increase of PFOA concentrations, there is an increase in the S value. Based on the current preliminary results, for the UIO-66-NH2-based device, a calibration curve of S = 8.28 * Con (ng/L) + 7.03; R2 = 14.83 is obtained, with a detection limit of ~ 35 ng/L. More work still needs to be done for the UIO-66-NH2-based device.

5.2.3 PFOA Water Sample Detection Based on MIL-101 (Cr) packed NP-µFEC

MIL-101(Cr) packed NP-µFEC device was tested with spiked water sample containing PFOA at 50 ng/L. The results are provided in Figure 14. The results show that sensors based on Cr-MIL-101 are also sensitive to the presence of PFOA. Hence Cr-MIL-101 based PFAS sensors will lack selectivity between PFOS and PFOA.

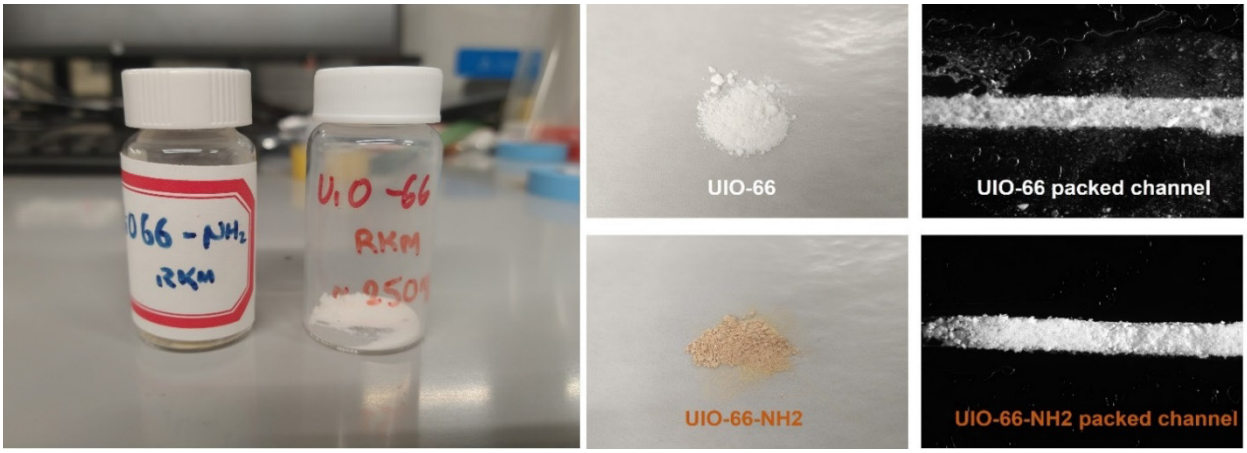

Figure 12. Picture of UIO-66 and UIO-66-NH2 and Their Corresponding optical Images of Packed Channel of NP-µFEC.

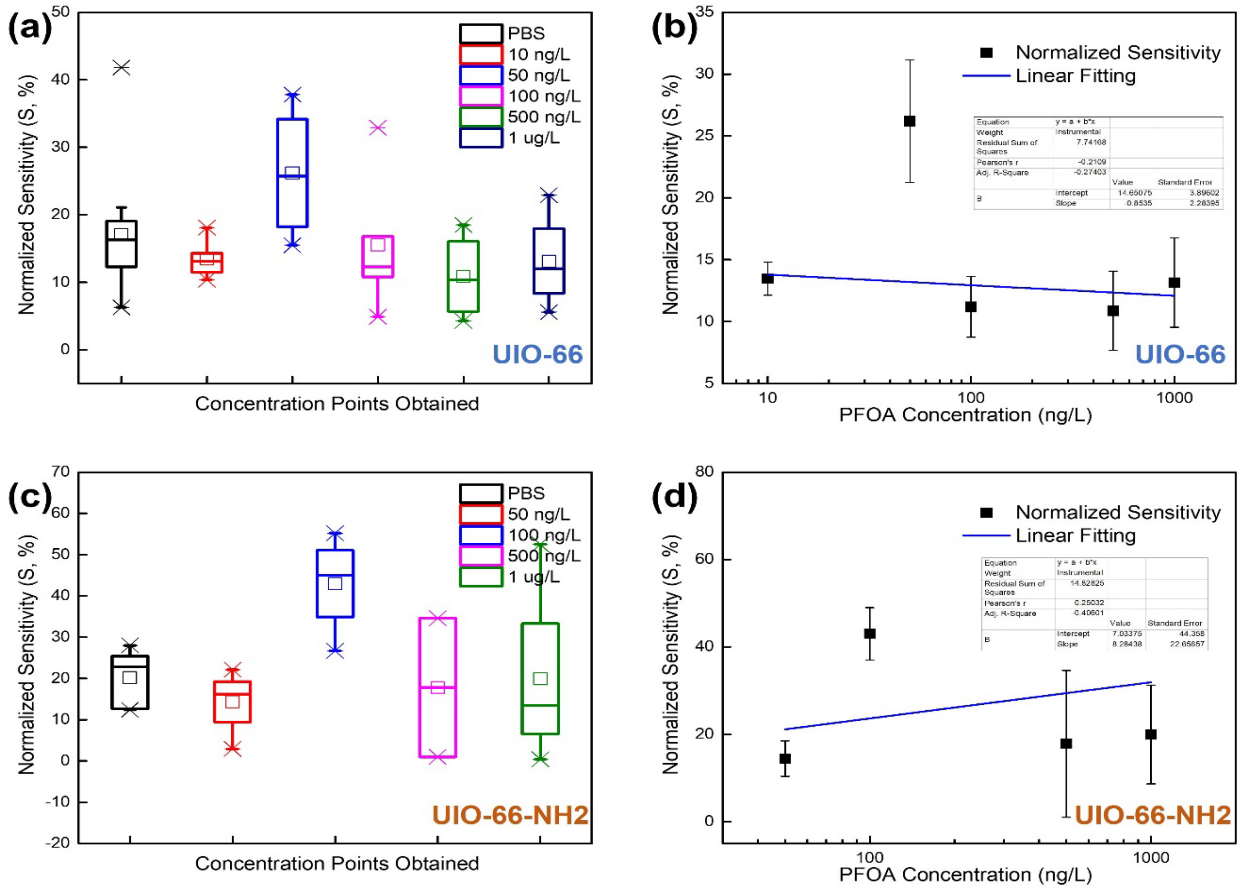

Figure 13. a) Box Plot Statistical Results for Different PFOA Concentrations and their Corresponding S Based on the UIO-66 Packed NP-μFEC Device. (b) Corresponding Calibration Curve for the Figure (a). (c) Box Plot Statistical Results for Different PFOA Concentrations and their Corresponding S Based on the UIO-66-NH2 Packed NP-μFEC Device. (d) Corresponding Calibration Curve for the Figure (c).

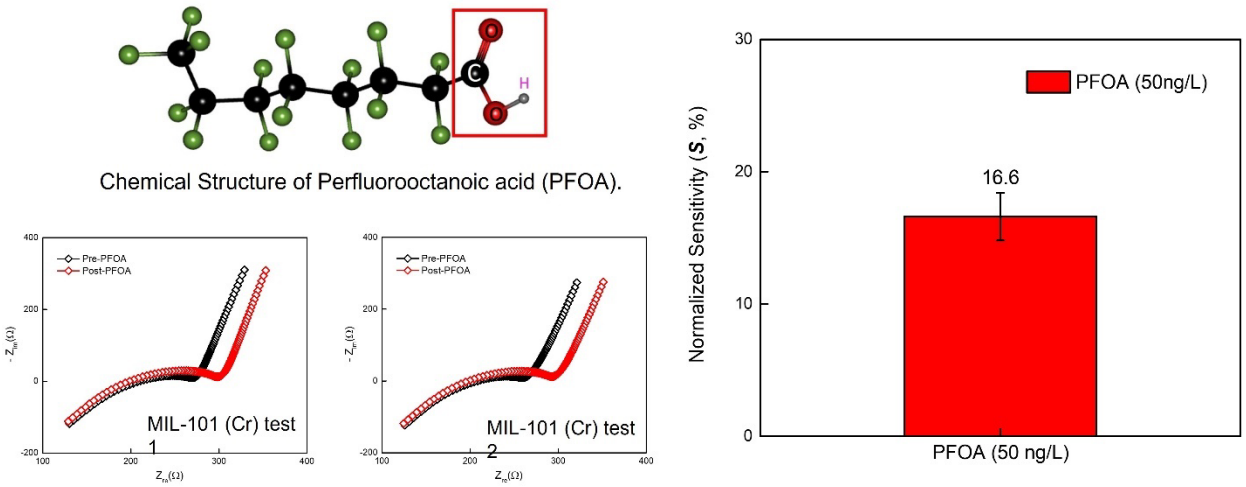

Figure 14. PFOA (50ng/L) Testing Results Based on Old MIL-101(Cr)

5.2.4 Three Real Water Sample Detection Based on MIL-101(Cr) packed NP-μFEC

Based on the current device MIL-101(Cr) packed NP-μFEC (Figure 2) and previously obtained calibration curve data, three water samples were run as shown in Figure 15. Due to the high PFAS concentrations, the water samples are diluted using DI water. After the dilution, relevant PFOA and sulfur containing PFAS concentrations are shown in Figure 15(b). For each water sample, six repeat testing are done, and the obtained averaged sensitivity (***S***) is calculated based on the box plots, as shown in Figure 13(c). Finally, the relationship between these three water samples' related ***S*** and the previously obtained calibration curve data is shown in Figure 15(d). In short, from Figure 15(d), it is found that the current MIL-101(Cr) packed NP-μFEC transducer can show a high sensitivity to PFOA molecules and almost all sulfur-containing PFAS molecules. Therefore, it appears that the current device's selectivity needs further optimization. To evaluate this selectivity, PFOA was run with Cr-Mil-101.

In addition, Figure 15(c) shows a high variation in the ***S***. The manual packing process is the likely reason for this variability. To explain, three possible equivalent circuits under different conditions are shown in Figure 16. If packing is loose and variable, electrical charges transferring to the external circuit will result through two possible pathways: (i) directly through the μEs to the external circuit; (2) the charges will go along the framework of the MOFs reach the μEs and then to the external circuit. Since each time it is difficult to control or achieve identical packing morphology, this will result in different MOF coverage to μEs. In other words, each time the exposed area of one μEs array to the electrolyte is different. Therefore, this will result in the element values in the red highlighted circuit being different (middle equivalent circuit); however, the valuable information needed is the changes in the Rct itself. The changes in the packing will directly determine the difficulty of observing the changes in Rct. Therefore, this is the most likely reason why there is a relatively high variation in the ***S*** for water sample data.

6.0 ACCURACY, PRECISION, AND QUALITY CONTROL ASSESSMENT

A double-blind accuracy, precision, and quality control (QC) test was performed to assess the precision and accuracy of the current PFAS sensor prototype and was coordinated by Arcadis. The QC test consisted of sending blind PFOS standards in the concentration range of 1 to 150 ng/L along with a DI water blank to NJIT and Pace Analytical lab (Pace). The PFOS standards (15, 47 and 75 ng/L) and the DI water blank were prepared at the Arcadis Treatability Laboratory in Durham, NC. The concentrations were not shared (i.e., prepared as "blind" samples") with either NJIT or Pace.

The 47 ng/L PFOS standard was divided into six parts (i.e., identical split samples), with five sent to NJIT and one sent to Pace. Similarly, the 15 ng/L PFOS standard was divided into three parts with two sent to NJIT and one to Pace lab. The 75 ng/L PFOS standard and the DI water blank were divided into two parts each and one part each was sent to NJIT and Pace lab. Hence a total of nine samples were sent to NJIT and four samples were sent to Pace lab. Different concentrations were included to assess accuracy whereas multiple samples of the same concentration were included to check precision. Pace lab used direct injection LC-MS/MS (Liquid Chromatography with tandem mass spectrometry) analysis for analyzing the standards and had an LOQ of 10 ng/L for PFOS.

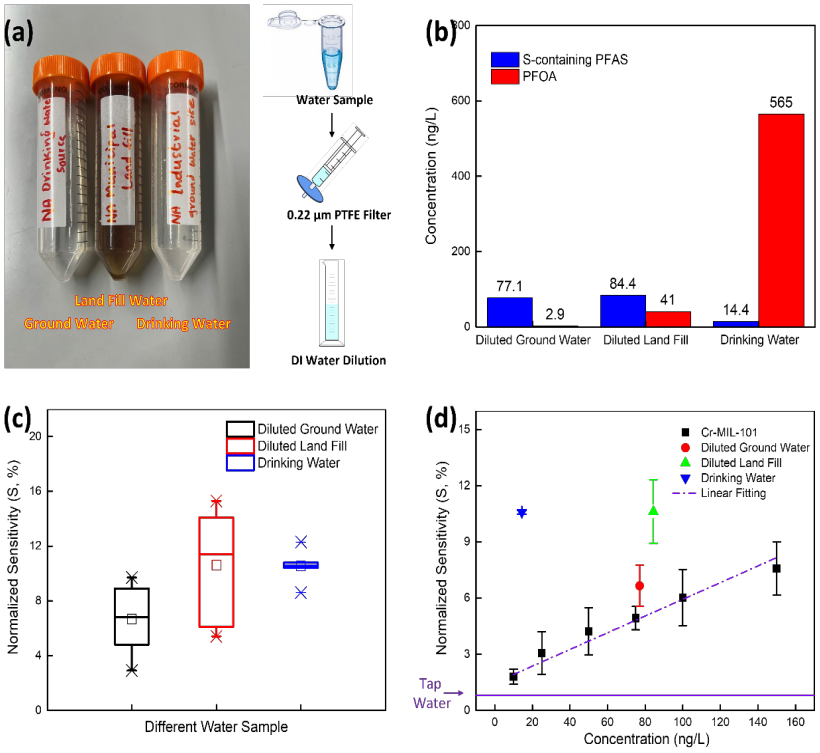

Figure 15. (a) Picture of Three Different Water Samples (Right) and Relevant Treatment Scheme for the Water Samples Before Testing (Left). (b) Concentrations of Sulfur-containing PFAS Molecules and PFOA in Each Treated/Diluted Water Sample. (c) Box Plot Statical Results for Each Water Sample and Corresponding S. (d) Calibration Curve of Cr-MIL-101 (Cr) Packed NP-µFEC to PFOS Spiked Tap Water Solutions and the Distribution of Calculated Averaged S to Each Water Sample.

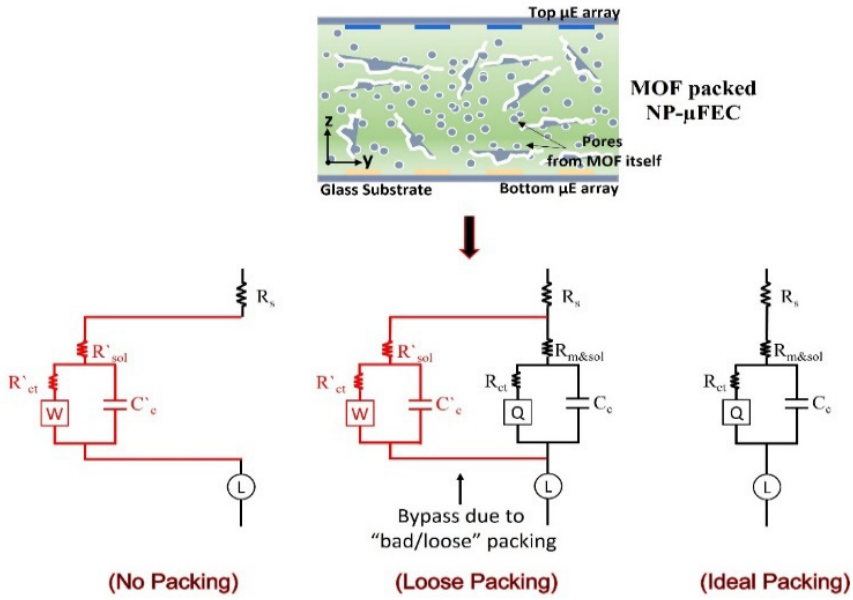

Figure 16. Possible Equivalent Circuits for MOF Packed NP-µFEC Device Under Different Configurations (a) No Packing; (b) "Bad/Loose" Packing; (c) Ideal Packing.

Because Pace lab did not detect PFOS in the 15 ng/L standards and NJIT's PFAS sensor leaked during the analysis of one of the 15 ng/L standards (PFOS Standard 7), these standards were not considered for assessing the precision and accuracy of the sensor. A comparison of the results from this assessment are shown graphically in Figure 17.

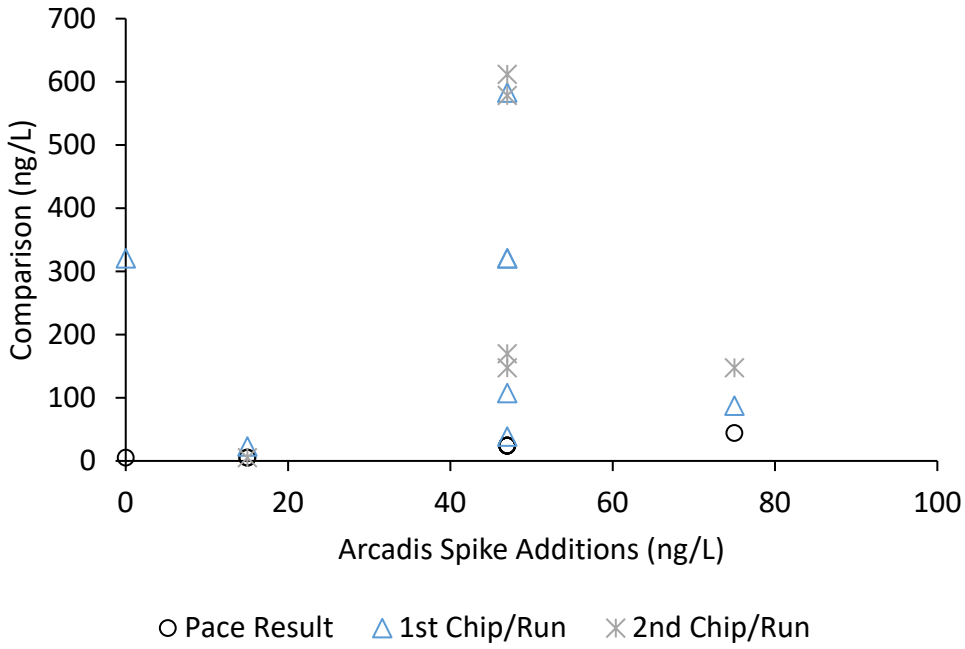

Figure 17. A Comparison of the Results from the Accuracy, Precision, and QC Assessment

For the assessment, the results from Pace were considered as the actual concentration and the PFAS sensor detections were compared to these results. The sensor results from NJIT, LC-MS/MS analysis results from Pace, and the standard deviation of each sensor result from the corresponding Pace lab result is given in Table 2. From the results, it can be seen that for the 47 ng/L PFOS standards, the PFAS sensor results from NJIT ranged from 102 to 580.7 ng/L. This corresponds to 429 to 2420% of the Pace lab result with a standard deviation 56 to 394 ng/L from the Pace result. In the case of precision, the standard deviation among the PFAS sensor results for the 47 ng/L standards was 229 ng/L corresponding to a relative standard deviation (RSD) of 83%.

For the 75 ng/L PFOS standard, the PFAS sensor showed a result of 117.3 ng/L which was 267% of the Pace lab result and had a standard deviation of 52 ng/L. Finally, for the DI water blank the PFAS sensor showed a PFOS concentration of 140.7 ng/L while the Pace lab did not detect any PFOS.

Table 2. Compiled results from the double-blind QC test conducted to assess the accuracy and precision of the PFAS Sensor

Sample Label	Expected PFOS Conc. (ng/L)	Pace LC-MS/MS Results (ng/L)	NJIT PFAS Sensor results (ng/L)	Standard Deviation (ng/L)
PFOS Standard 1	15	ND	14	-------
PFOS Standard 2	47	24	580.7	393.6
PFOS Standard 3	47	24	104	56.6
PFOS Standard 4	75	44	117.3	51.8
PFOS Standard 5	47	24	127.3	73.0
PFOS Standard 6	47	24	466.2	312.7
PFOS Standard 7	15	ND	-------	-------
PFOS Standard 8	DI water blank	ND	140.7	--------
PFOS Standard 9	47	24	102.9	55.8

*ND- Not Detected

Key performance objectives specifically related to sensor accuracy and precision were provided in the original proposal, the Spring 2022 Interim Progress Report meeting, and also in a White Paper provide to ESTCP in June 2002. In general, it was expected that the sensor would exhibit an accuracy approximately equivalent to an ELAP-certified laboratory and an analytical precision (i.e., repeatability) of less than +/- 30%. Furthermore, it was expected that the sensor would achieve a performance variation of less than 20% difference for a range of water matrices (i.e., variable pH, ionic strength, hardness, and co-contaminants such as DOC and other PFASs). Based on the results obtained to-date, it is clear that the accuracy and precision of the sensor varied substantially from the accuracy and precision targets. Furthermore, the team has discussed significant error analysis and troubleshooting options and believes that current sensor design cannot come close to achieving any of these criteria. Therefore, a No-Go for the remainder of project activities was recommended. Hence the sensor performance in field samples and the planned field demonstration was not performed.

7.0 ADDRESSING STRUCTURAL HETEROGENEITY OF CR-MIL-101

One of the reasons for high variations in the sensitivity readings at the same target PFAS concentration in due to heterogeneity of particle size in the MOFs used. MOF structural variability or heterogeneity can exist between synthesis batches, where (i) the particle sizes and (ii) pore characteristics (surface area, pore volume) might vary. After observing the lack of precision in PFAS measurements during H1 CY2022, PNNL identified particle size distribution as one potential source of variability and uncertainty in the sensor measurements. In order to better understand this issue, PNNL made internal investments to characterize the particle size distribution of a Cr-MIL-101 MOF batch. The MOF was dispersed in ethanol before and after ball milling wash. Figure 18 shows the following:

- Before ball milling, the Cr-MIL-101 MOF particles had broadly distributed particle sizes from 0.2- 100 µm.
- After ball milling for 2h, we observed a bimodal particle size distribution. One peak is between 0.1-10 µm and another between 20-500 µm.
- After ball milling the MOFs for 2 days, the particle size distribution remains bimodal. Still, a smaller peak of particles was observed between 0.1-1 µm and a larger peak of aggregated particles between 20-500 µm.

The Cr-MIL-101 MOF, after 48h of ball-milling (bimodal particle size distribution, yellow curve in Figure 17), was separated using centrifugation. By centrifuging the MOF samples at high RPM first, followed by supernatant separation and centrifuging again at low RPM, we obtained were able to obtain a much more uniform particle size distribution, as shown in Figure 19. This ball-milling procedure, or one like it, will be used to avoid particle size heterogeneity in future experiments.

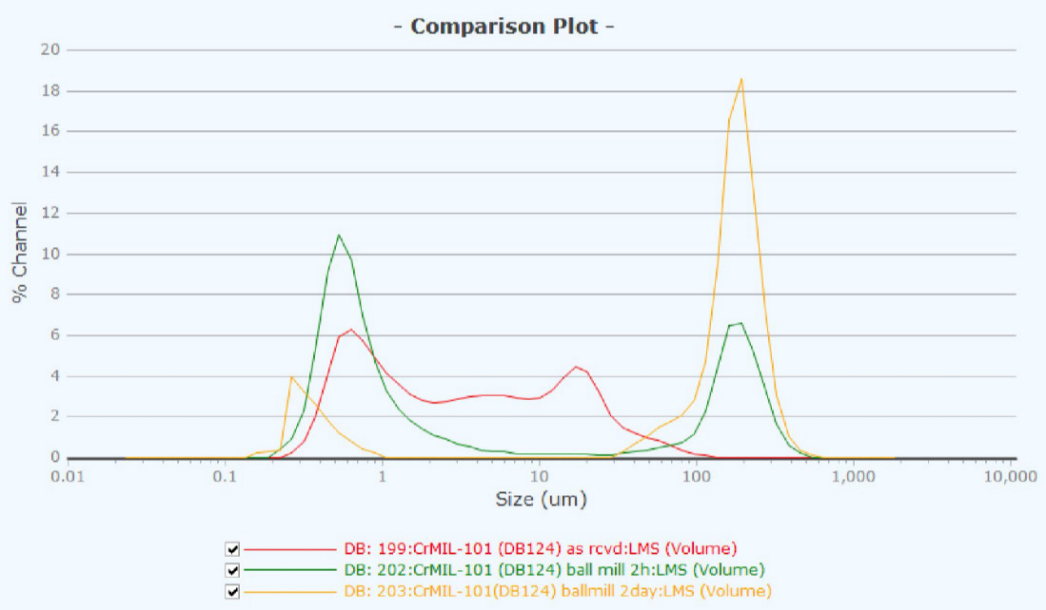

Figure 18. Ball Milling of Cr-MIL-101 in an Ethanol Solution, as Received (Red), After 2h (Green) and After 48h (Yellow)

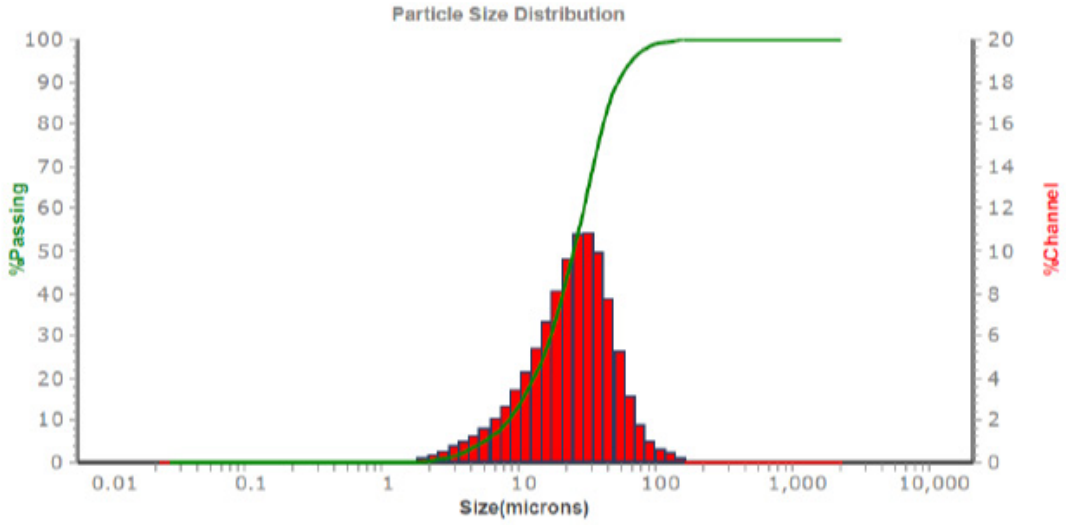

Figure 19. Cr-MIL-101, After Ball-milling for 48h in an Ethanol Solution, Followed Centrifuging of the Samples at High RPM First, Followed by Supernatant Separation and Centrifuging Again at Low RPM

8.0 IMPLEMENTATION ISSUES

Based on the bench-scale laboratory tests conducted, the following lessons learned can be applied during future PFAS sensor research.

- The Cr-MIL-101 based sensor lacked selectivity between PFOA and PFOS
- The sensor failed to achieve an accuracy similar to an ELAP-certified lab and precision of +/- 30%.
- The variation of MOFs within and between batches needs to be minimized. The variation is mainly caused by the large variation in particle size distribution. This particle size heterogeneity could be avoided by using the ball milling process optimized by PNNL for future batches.
- Packing of MOFs in the sensor needs to be optimized to maintain accuracy and precision between sensors. Manual packing, a potential source of variation between sensors, needs to be avoided. Additionally, a larger sensor footprint is recommended to achieve a leak proof design and homogenous packing.

9.0 REFERENCES

Barpaga, D.; Bahattacharya, P.; Garburu-Carusso, V.; Chatterjee, S.; Motkuri, R. K., Capture selectivity of porous sorbents towards PFASs. *Chemical Communications* **2019**, In preparation.

Barpaga, D.; Zheng, J.; Han, K. S.; Soltis, J. A.; Shutthanandan, V.; Basuray, S.; McGrail, B. P.; Chatterjee, S.; Motkuri, R. K., Probing the Sorption of Perfluorooctanesulfonate Using Mesoporous Metal–Organic Frameworks from Aqueous Solutions. *Inorganic chemistry* **2019,** *58* (13), 8339-8346.

Barzen-Hanson, K. A.; Roberts, S. C.; Choyke, S.; Oetjen, K.; McAlees, A.; Riddell, N.; McCrindle, R.; Ferguson, P. L.; Higgins, C. P.; Field, J. A., Discovery of 40 Classes of Per- and Polyfluoroalkyl Substances in Historical Aqueous Film-Forming Foams (AFFFs) and AFFF-Impacted Groundwater. *Environ Sci Technol* **2017,** *51* (4), 2047-2057.

Berger, U.; Haukas, M., Validation of a screening method based on liquid chromatography coupled to high-resolution mass spectrometry for analysis of perfluoroalkylated substances in biota. *J Chromatogr A* **2005,** *1081* (2), 210-217.

Bower, J. K.; Barpaga, D.; Prodinger, S.; Krishna, R.; Schaef, H. T.; McGrail, B. P.; Derewinski, M. A.; Motkuri, R. K., Dynamic Adsorption of CO2/N2 on Cation-Exchanged Chabazite SSZ-13: A Breakthrough Analysis. *ACS Appl Mater Interfaces* **2018,** *10* (17), 14287-14291.

Cahill, P. S.; Walker, Q. D.; Finnegan, J. M.; Mickelson, G. E.; Travis, E. R.; Wightman, R. M., Microelectrodes for the measurement of catecholamines in biological systems. *Anal Chem* **1996,** *68* (18), 3180-3186.

Chatterjee, S.; Motkuri, R. K.; Basuray, S. Microfluidic impedance platform for in-situ detection and quantification of PFASs in groundwater. PNNL-IPID: 31421-E. May, 2020.

Chatterjee, S.; Norton, A. E.; Edwards, M. K.; Peterson, J. M.; Taylor, S. D.; Bryan, S. A.; Andersen, A.; Govind, N.; Albrecht-Schmitt, T. E.; Connick, W. B., Highly Selective Colorimetric and Luminescence Response of a Square-Planar Platinum (II) Terpyridyl Complex to Aqueous TcO4–. *Inorganic Chemistry* **2015,** *54* (20), 9914-9923.

Chen, S. H.; Li, A. M.; Zhang, L. Z.; Gong, J. M., Molecularly imprinted ultrathin graphitic carbon nitride nanosheets-Based electrochemiluminescence sensing probe for sensitive detection of perfluorooctanoic acid. *Anal Chim Acta* **2015,** *896*, 68-77.

Chen, L. D.; Lai, C. Z.; Granda, L. P.; Fierke, M. A.; Mandal, D.; Stein, A.; Gladysz, J. A.; Buhlmann, P., Fluorous Membrane Ion-Selective Electrodes for Perfluorinated Surfactants: Trace-Level Detection and in Situ Monitoring of Adsorption. *Anal Chem* **2013,** *85* (15), 7471-7477.

Chen, M.-J.; Yang, A.-C.; Wang, N.-H.; Chiu, H.-C.; Li, Y. L.; Kang, D.-Y.; Lo, S.-L., Influence of crystal topology and interior surface functionality of metal-organic frameworks on PFOA sorption performance. *Microporous and Mesoporous Materials* **2016,** *236*, 202-210.

Cheng, Y.-H.; Moura, P. A. R.; Zhenglong, L.; Feng, L.; Arokiam, S.; Yang, J.; Hariharan, M.; Basuray, S., Effect of electrode configuration on the sensitivity of nucleic acid detection in a non-planar, flow-through, porous interdigitated electrode. *Biomicrofluidics* **2019,** *13* (6), 064118.

Cheng, Y. H.; Barpaga, D.; Soltis, J.; Shutthanandan, V.; Kargupta, R.; Han, K. S.; McGrail, B. P.; Motkuri, R. K.; Basuray, S.; Chatterjee, S., Metal-Organic Framework Based Microfluidic Impedance Sensor Platform for Ultrasensitive Detection of Perfluorooctanesulfonate. *ACS Applied Materials & Interfaces* **2020**, 12(9), 10503-10514.

Defense, O. o. t. S. o., Investigating Per- and Polyfluoroalkyl Substances within the Department of Defense Cleanup Program. 2019.

Ding, S.; Mosher, C.; Lee, X. Y.; Das, S. R.; Cargill, A. A.; Tang, X.; Chen, B.; McLamore, E. S.; Gomes, C.; Hostetter, J. M., Rapid and label-free detection of interferon gamma via an electrochemical aptasensor comprising a ternary surface monolayer on a gold interdigitated electrode array. *Acs Sensors* **2017,** *2* (2), 210-217.

Gong, J. M.; Fang, T.; Peng, D. H.; Li, A. M.; Zhang, L. Z., A highly sensitive photoelectrochemical detection of perfluorooctanic acid with molecularly imprined polymer-functionalized nanoarchitectured hybrid of AgI-BiOI composite. *Biosens Bioelectron* **2015,** *73*, 256-263.

Hu, X. C.; Andrews, D. Q.; Lindstrom, A. B.; Bruton, T. A.; Schaider, L. A.; Grandjean, P.; Lohmann, R.; Carignan, C. C.; Blum, A.; Balan, S. A.; Higgins, C. P.; Sunderland, E. M., Detection of Poly- and Perfluoroalkyl Substances (PFASs) in U.S. Drinking Water Linked to Industrial Sites, Military Fire Training Areas, and Wastewater Treatment Plants. *Environ Sci Technol Lett* **2016,** *3* (10), 344-350.

Ji, W.; Xiao, L.; Ling, Y.; Ching, C.; Matsumoto, M.; Bisbey, R. P.; Helbling, D. E.; Dichtel, W. R., Removal of GenX and Perfluorinated Alkyl Substances from Water by Amine-Functionalized Covalent Organic Frameworks. *J Am Chem Soc* **2018,** *140* (40), 12677-12681.

Karimian, N.; Stortini, A. M.; Moretto, L. M.; Costantino, C.; Bogialli, S.; Ugo, P., Electrochemosensor for Trace Analysis of Perfluorooctanesulfonate in Water Based on a Molecularly Imprinted Poly(o-phenylenediamine) Polymer. *Acs Sensors* **2018,** *3* (7), 1291-1298.

Kaushik, A.; Yndart, A.; Kumar, S.; Jayant, R. D.; Vashist, A.; Brown, A. N.; Li, C.-Z.; Nair, M., A sensitive electrochemical immunosensor for label-free detection of Zika-virus protein. *Sci Rep-Uk* **2018,** *8* (1), 1-5.

Li, Z.; Cheng, Y.-H.; Feng, L.; Neil, J.; Antonio, R. M. P.; Rahman, M.; Yang, J.; Azizighannad, S.; Mitra, S.; Basuray, S., Communication—Electrochemical Impedance Signature of a Non-Planar, Interdigitated, Flow-Through, Porous, Carbon-Based Microelectrode. *Journal of The Electrochemical Society* **2019,** *166* (16), B1669.

Liu, K.; Zhang, S.; Hu, X.; Zhang, K.; Roy, A.; Yu, G., Understanding the Adsorption of PFOA on MIL-101(Cr)-Based Anionic-Exchange Metal-Organic Frameworks: Comparing DFT Calculations with Aqueous Sorption Experiments. *Environ Sci Technol* **2015,** *49* (14), 8657-65.

Mecker, L. C.; Filla, L. A.; Martin, R. S., Use of a Carbon-Ink Microelectrode Array for Signal Enhancement in Microchip Electrophoresis with Electrochemical Detection. *Electroanalysis* **2010,** *22* (19), 2141-2146.

Min, J.; Baeumner, A. J., Characterization and optimization of interdigitated ultramicroelectrode arrays as electrochemical biosensor transducers. *Electroanalysis: An International Journal Devoted to Fundamental and Practical Aspects of Electroanalysis* **2004,** *16* (9), 724-729.

Motkuri, R. K., et al. Compostion and method for capture and degradation of PFAS. PNNL-IPID: 31745-E. May, 2020.

Motkuri, R. K.; Chatterjee, S. Redox-Active Nanoporous Capture Probe Based Electrochemical Affinity Sensors for Ultrasensitive PFAS Detection. Provisional Patent. EFS ID# 37904470; Application # 62942637; Confirmation #1045. . December 2, 2019.

Motkuri, R. K.; Annapureddy, H. V.; Vijaykumar, M.; Schaef, H. T.; Martin, P. F.; McGrail, B. P.; Dang, L. X.; Krishna, R.; Thallapally, P. K., Fluorocarbon adsorption in hierarchical porous frameworks. *Nat Commun* **2014,** *5*, 4368.

Sini, K.; Bourgeois, D.; Idouhar, M.; Carboni, M.; Meyer, D., Metal–organic framework sorbents for the removal of perfluorinated compounds in an aqueous environment. *New Journal of Chemistry* **2018,** *42*, 17889-17894.

USEPA. (2022). *Drinking Water Health Advisories for PFAS- Fact Sheet for Communities*.

Weiss-Errico, M. J.; Ghiviriga, I.; O'Shea, K. E., F-19 NMR Characterization of the Encapsulation of Emerging Perfluoroethercarboxylic Acids by Cyclodextrins. *J Phys Chem B* **2017,** *121* (35), 8359-8366.

Wightman, R. M., Probing cellular chemistry in biological systems with microelectrodes. *Science* **2006,** *311* (5767), 1570-1574.

Zhang, C. H.; Hopkins, Z. R.; McCord, J.; Strynar, M. J.; Knappe, D. R. U., Fate of Per- and Polyfluoroalkyl Ether Acids in the Total Oxidizable Precursor Assay and Implications for the Analysis of Impacted Water. *Environ Sci Tech Let* **2019,** *6* (11), 662-668.

Zheng, J.; Barpaga, D.; Gutierrez, O. Y.; Browning, N. D.; Mehdi, B. L.; Farha, O. K.; Lercher, J. A.; McGrail, B. P.; Motkuri, R. K., Exceptional Fluorocarbon Uptake with Mesoporous Metal-Organic Frameworks for Adsorption-Based Cooling Systems. *Acs Applied Energy Materials* **2018,** *1* (11), 5853-5858.

Zheng, J.; Vemuri, R. S.; Estevez, L.; Koech, P. K.; Vargas, T.; Camaioni, D. M.; Blake, T. A.; McGrail, B. P.; Motkuri, R. K., Pore-Engineered Metal-Organic Frameworks with Excellent Adsorption of Water and Fluorocarbon Refrigerant for Cooling Applications. *Journal of the American Chemical Society* **2017,** *139* (31), 10601-10604.

Zheng, J.; Barpaga, D.; Trump, B. A.; Shetty, M.; Fan, Y.; Bhattacharya, P.; Jenks, J. J.; Su, C.-Y.; Brown, C. M.; Maurin, G.; McGrail, B. P.; Motkuri, R. K., Molecular Insight into Fluorocarbon Adsorption in Pore Expanded Metal–Organic Framework Analogs. *J Am Chem Soc* **2020,** *142* (6), 3002-3012.